INVESTIGATING VIBRATIONAL HEAT CAPACITIES OF GAS-PHASE BIOMOLECULAR IONS FOR USE IN DETERMINING ION THERMOCHEMISTRY

by

LAWREN R. PARIS

A THESIS

Presented to the Department of Chemistry and Biochemistry
and the Robert D. Clark Honors College
in partial fulfillment of the requirements for the degree of
Bachelor of Science

May 2024

An Abstract of the Thesis of

Lawren R. Paris for the degree of Bachelor of Science
in the Department of Chemistry and Biochemistry to be taken June 2024

Title: Investigating Vibrational Heat Capacities of Gas-Phase Biomolecular Ions for Use in Determining Ion Thermochemistry

Approved: *Dr. James S. Prell*
Primary Thesis Advisor

As the field of native mass spectrometry grows, there is increasing interest in quantitatively determining ion dissociation, unfolding thermochemistry, and kinetics using commonly available mass spectrometers. In particular, understanding the relationship between ion activation, internal energy, and temperature will likely be necessary for detailed structural interpretation of Collision Induced Dissociation and Collision Induced Unfolding data for native biomolecular ions and their complexes. Here, we use quantum computational theory to predict heat capacities for a variety of model biomolecular structures and report effects of level of theory, basis set, ion secondary structure, and biomolecule type on vibrational heat capacity per vibrational degree of freedom from 100 to 3000 K. On a degree-of-freedom basis, these values are remarkably invariant within each biomolecule type and can be used to estimate heat capacities of much larger biomolecular ions. We also explore effects of heat capacity ion heating, cooling, and internal energy distribution as a function of time use a home-built program (IonSPA). We observe that these internal energy distributions can be nearly Boltzmann for larger ions and at higher temperatures achieved through collisional heating after a brief (few-μs) induction period.

Acknowledgements

I would like to thank my research advisor, Dr. Jim Prell, for his four years of guidance and mentorship. His continued support and teaching allowed me to find confidence in my abilities and take ownership of my own research project. I have grown immensely through the 4 years I have spent in lab, and learned so much about myself through the process of writing this thesis and the accompanying paper for publication. Thanks to Dr. Lindsay Hinkle for her help in revising this thesis and for serving on my thesis committee.

A big thank you as well to my graduate student mentors and the entirety of the Prell lab, especially Dr. Sam Shepherd. Sam was always there to brainstorm ideas or help explain concepts I was struggling with, and made me feel extremely welcome in the lab. I could not have asked for a better mentor. I would also like to thank my fellow undergraduates in the lab, Lily Miller, Maria Soto-Cuesta, and Jacob Koscho for their friendship, guidance, and for letting me complain about my workload constantly.

I am so grateful to the Hui family, who supported me financially through the Hui Undergraduate Scholars Program, and to the American Society for Mass Spectrometry for their travel scholarship and for allowing me to present my work at their annual conference. I would not have made it without their financial support.

A huge thank you to my roommates and friends, who have supported me throughout my time in undergraduate and encouraged me to follow my passions. To my roommates and best friends, Eme and Maggie, thank you for helping me push myself and for sticking by me when I needed you most. To all my other friends, I am so grateful to have you as a supportive network. I could not have done this without you.

Finally, to my family. Thank you for believing in me, showing excitement in my research and passions even when you couldn't understand them, and for encouraging me to be curious about the world. You helped to develop this passion for science and chemistry, and I cannot thank you enough. Thank you for being there for all the good and bad moments that came with this project. I love you!

Table of Contents

List of Figures

List of Tables

Introduction

Basics of protein analysis

Proteins are biomolecular polymers made up of differing combinations of amino acids, which serve various biological functions. There exist hundreds of thousands of proteins in the human body, each of which plays a large role in cell regulation, duplication, and the immune system, to name only a few examples.[1] The vast majority of disease-regulatory drugs work by targeting specific sites on proteins, called active sites.[1] Based on the configuration of the active site, a molecule must be engineered so that it will preferably bind to that site and either slow down, speed up, or otherwise modify the protein's reactivity.[1] While the structures of some proteins, and thus their active sites, are relatively well understood, many proteins and protein complexes have not yet been characterized. In addition, when proteins are exposed to stressors like high or low temperature or pH, they may denature or dissociate into component parts, causing them to lose their ability to perform their intended function. By deliberately unfolding a protein and simultaneously measuring its thermochemical and/or kinetic properties, we can often infer information about the folded, or "native" state of the protein.[2,3] Developing new methods to observe unfolding processes and their associated thermodynamics and kinetics applicable to a wide variety of proteins, then, holds great promise for drug development and disease characterization.

Common techniques of protein analysis

Each of the most widely-used current methods of analyzing protein structure and activity has its own strengths and weaknesses. X-ray crystallography uses x-ray diffraction on crystallized samples to create a map of areas with high and low electron density based on those

diffraction patterns.[4] An atomically-resolved structure of the crystallized molecule is determined based on those regions of high or low density.[4] As a technique, X-ray crystallography is suitable for any protein that can crystallize in its native state, but can be challenging with many other proteins, such as membrane proteins (which require a membrane-like environment to remain stable) or intrinsically disordered proteins.[4] Some proteins also do not readily crystallize in their native state, and the process of crystallization may alter the native structure or purify out a single structure while leaving other structures behind in the crystallization solvent. Another common technique is cryogenic electron microscopy (CryoEM). In CryoEM, the biological sample in question is frozen in place using liquid ethane and kept cold inside the instrument with liquid helium or nitrogen, and an image of it is acquired using an electron microscope at many different angles.[5] These 2-dimensional images are then compiled to create a 3D model of the structure of the sample.[5] This technique can be difficult to use for characterizing highly heterogeneous proteins, as well as those smaller than 50 kDa.[5] Nuclear Magnetic Resonance, or NMR, can also be used to determine atomically-resolved protein structures. The quantum spin of protons and neutrons creates a magnetic field within the nuclei of the atoms in a molecule, and by applying an external magnetic field, the atoms may be excited to a higher energy level.[6] Once this field is turned off, the atoms relax back to their ground state, and release energy, which is then recorded by a detector.[6] NMR may be used for a specific type of atom, typically proton NMR or carbon NMR, to identify the number of atoms and their placement within the molecule.[6] This technique is extremely challenging for proteins with masses above ~20 kDa, making it not suitable for analysis of many important biological proteins. Native Ion Mobility-Mass Spectrometry (nIM-MS), is a gas-phase technique for studying biomolecule structure that addresses many of the above challenges.[2]

Native Ion Mobility Mass Spectrometry (nIM-MS)

Native Ion Mobility-Mass Spectrometry (nIM-MS) is a form of mass spectrometry in which the biomolecular ions studied inside the instrument have structures as close as possible to their solution-phase folded, or "native", state.[2,7] A diagram of a Waters Synapt G2S*i*, an example of a commercial instrument widely used to perform nIM-MS experiments, can be found in Figure 1.[8] In typical nIM-MS experiments, a sample containing a biomolecule or biomolecular complex of interest, such as a protein, is buffer-swapped into a volatile buffer, commonly ammonium acetate, with the same pH and ionic strength as the original buffer (often Tris, phosphate buffer, HEPES, or other common biochemical buffers).[2] After loading ~5 μL of the buffer-swapped sample into a capillary tube with a ~1-micron wide opening, a wire is inserted into the sample solution inside the capillary, which is then placed in front of the source of the instrument.[2] When a voltage of several hundred volts is applied to the wire, micron-sized or smaller electrically charged droplets of solvent containing the protein are emitted from the capillary and are drawn into the source cone of the mass spectrometer.[2] This process is known as electrospray ionization.[2,9,10] These charged droplets evaporate extremely quickly (nanosecond to microsecond time scale), leaving charged gaseous ions of the protein in its native state to travel through the instrument.[2,10] Once the ions with various charges travel through the instrument and hit the ion detector, a signal is produced that shows the abundance of ions for each mass/charge ratio (m/z).[2] Based on the spacing between consecutive peaks in the mass spectrum, as well as the m/z values at those points, it is possible to determine the consecutive charge states of each ion, as well as their masses and abundances, and determine the abundant oligomeric states of the protein.[2] The mass of the ion can often be determined to just a few parts-per-million, which is often enough to distinguish different proteins with very similar masses or even precisely

determine the number and types of adducts, ligands, and/or post-translational modifications on a protein.[2] Another useful consequence of these sensitive mass measuring capabilities is that if a protein is commonly found as a dimer, where two protein monomers come together to form one protein complex, mass spectrometry can detect this information.[2,7] For example, if two or more proteins in the body naturally form dimeric or multimeric complexes, this can affect how drugs can be developed to target these proteins, so this information is extremely useful in biological and pharmaceutical research. This information can be much more directly determined using nIM-MS, which uses the protein in its native state, than with other common types of MS that use denatured or digested biomolecular samples.

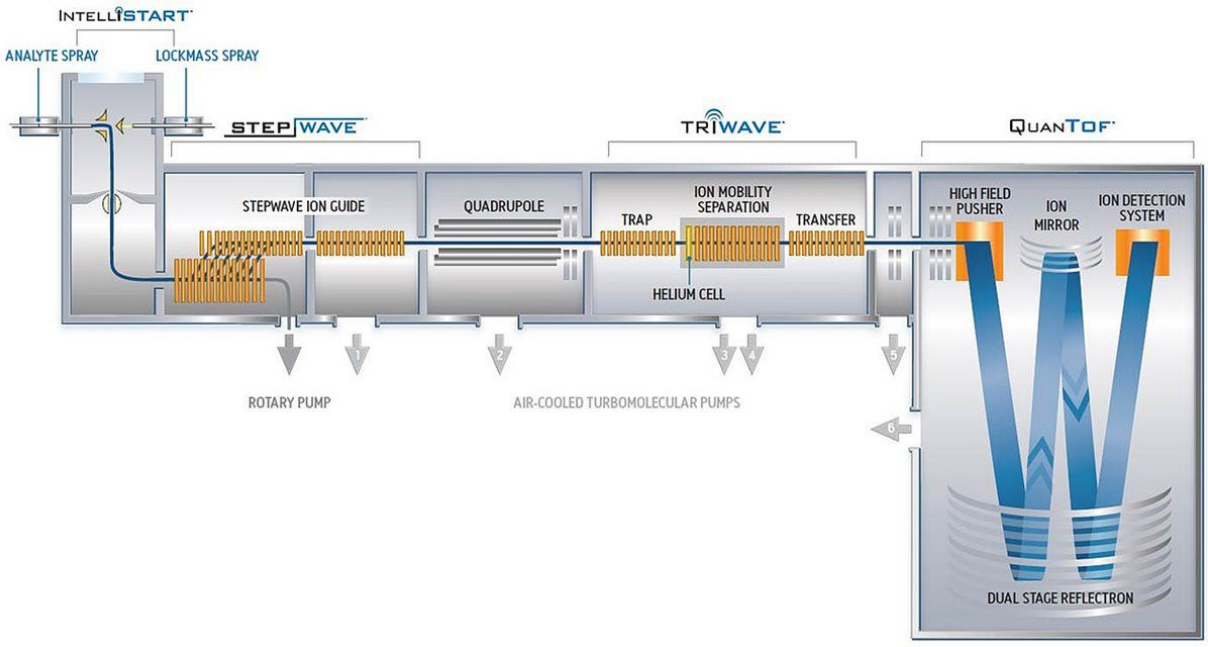

Figure 1. Annotated diagram of a commercial mass spectrometer (Waters Synapt G2S*i*).[8]

Collision Induced Dissociation/Unfolding experiments

To extract more useful information from nIM-MS, researchers often make use of Collision Induced Dissociation (CID) and Collision Induced Unfolding (CIU). Both techniques require use of an instrument that includes a region, called a "collision cell", where the ions collide with a neutral buffer gas in order to heat them.[10] The ions are accelerated towards this collision cell using a relatively high (10's to 100's of volts) electric potential.[2,10] The collision cell is filled with neutral gas molecules, typically helium, argon, or nitrogen gas.[2] When the ions enter the collision cell, they collide with hundreds to many thousands of neutral gas particles.[2,3,10] Some of the kinetic energy they obtained from being accelerated transforms into internal energy with each collision, and the increased internal energy of the ion can eventually lead to fragmentation ("dissociation") of the protein ion.[3,10] After fragmentation, the fragment ions as well as any remaining un-fragmented ions travel into another mass analyzer, where their m/z is measured.[3] This additional step of analysis after fragmentation allows for greater insight into which parts of the molecule are bound more tightly and which are bound loosely.

CIU experiments are very similar to CID experiments, except that only enough energy is added to the protein by collisions to disrupt non-covalent bonds holding its tertiary structure together, leading to unfolding of some or all of the ion, rather than fragmentation into pieces.[2,10] Because the m/z of the unfolded ion is the same as that of the original, native ion, an additional type of separation is needed to determine what fraction of the ion population has unfolded.[10] Ion mobility separation can be used for this purpose. In this technique, ions are pulsed into a tube of buffer gas at ~100 times the pressure used for CID, and a gentle electric field is used to pull the ions from one side of the tube to the other.[2] These conditions do not tend to cause further fragmentation or unfolding of the ion, but instead cause ions of different shape or overall size to

separate from one another in time and space, akin to a balled-up piece of paper dropping through air to the floor as compared to a flat sheet of paper.[2,10] An important feature of ion mobility separation is that native and unfolded protein ions can not only be separated from one another and quantified, but the time it takes them to traverse the ion mobility tube (their "drift times") can be used to determine their physical shape and size in the form of a "collision cross section", analogous to their rotationally-averaged "shadow".[2,10] By plotting an ion's drift time (or collision cross section) against the injection potential used to unfold it in the collision cell, a CIU "fingerprint" can be obtained. A typical CIU "fingerprint" plot for Bovine Serum Albumin (BSA) can be found in Figure 2. Here, the y-axis represents the ion's drift time, and the x-axis is the collision voltage, which is related to amount of energy given to the ions during the collision phase and affects how readily the ion is dissociated or unfolded.[10] As shown in the spectra in Figure 2, CIU fingerprints commonly appear as several horizontal bands. Each of these bands (labeled below as 1, 2, 3, 4) represents a transitional state of the molecule as it unfolds more and more. Each step requires more collision energy before the molecule has enough energy to go through a transition into a subsequent state, and each unfolding state of the molecule has a different drift time through the instrument, which allows these states to be differentiated and detected.[7,11] A major goal of the Prell research group is to determine how one can work backwards from these CIU fingerprints to determine the way in which the protein was folded in its native state.

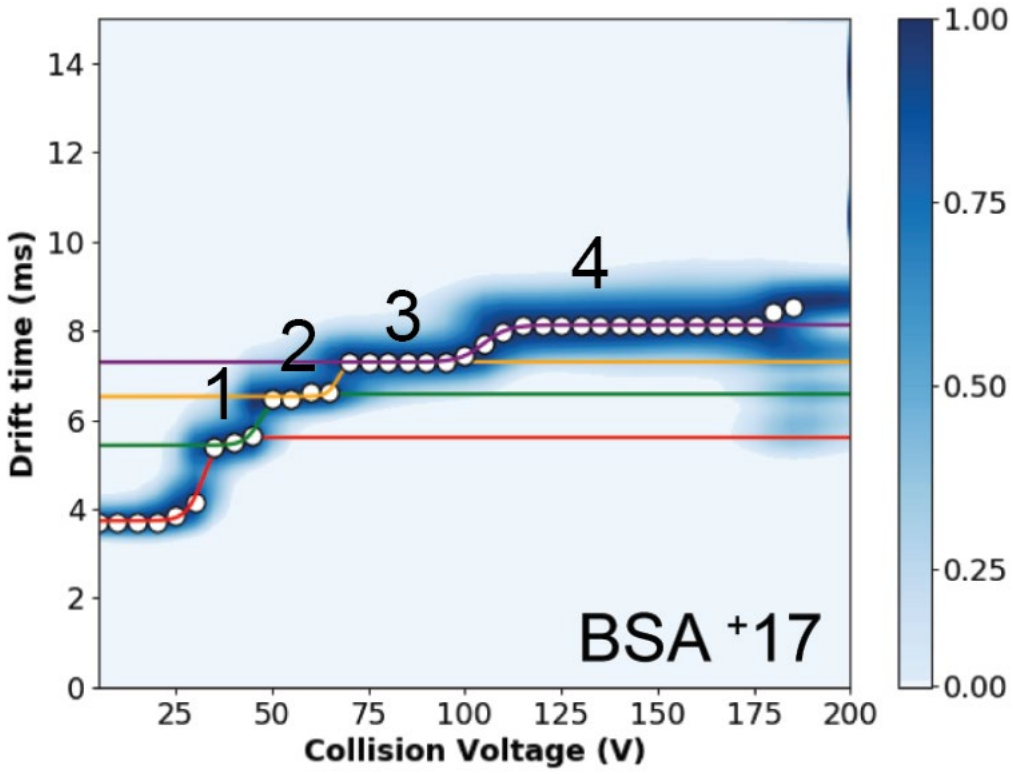

Figure 2. Annotated CIU fingerprint for Bovine Serum Albumin 17+ charge state

nIM-MS can be highly useful for protein and biomolecule analysis

Because proteins and other biomolecules travel through the instrument in their native state, nIM-MS offers additional structural information that is not able to be resolved or quantified using other biomolecular analysis techniques.[2] Beyond mass measurement, CIU and CID experiments can provide further information on the mechanisms of unfolding or dissociation for a given biomolecular ion, allowing scientists to infer more details about native state structure.[10] In addition, nIM-MS is a relatively fast technique, as gas-phase unfolding in CID/CIU experiments takes place at the microsecond scale, and high-quality CID breakdown curves and CIU fingerprints can be acquired on the order of tens of minutes.[10] The low sample requirements (typically, a few microliters of solution at micromolar concentration, i.e., nanomoles or less of the protein analyte) are another reason why nIM-MS can be a preferential

technique for many experiments. As described previously, only approximately 5 μL or less of sample is required, which allows for many more experiments to be run with the same sample. Capable of handling ions with masses from a few hundred Da to at least ~20 MDa, nIM-MS also works well for proteins in the ranges where other techniques fall short.[2] Many proteins with molecular weights in between the ideal ranges for NMR and CryoEM can still be easily characterized by nIM-MS, and proteins that do not easily crystallize in their native state or are highly heterogeneous are also able to be analyzed successfully using this technique.[2] Used in tandem with other more prevalent techniques, nIM-MS is a powerful tool for understanding protein unfolding and dissociation mechanics while still being fast, accessible, and accurate.

Thermochemistry from nIM-MS analysis: Gibbs free energy, transition state entropy, transition state enthalpy

By utilizing nIM-MS and CID/CIU, many important thermochemical and kinetic values can be obtained that, in principle, may provide information about the gas-phase structure of the native ion and its parent solution-phase structure.[7] Activation energy refers to the amount of energy required to overcome an energy barrier for a reaction.[12] To find the activation energy of the transition, the slope of a linear fit of the following equation can be used, where *A* represents the Arrhenius constant (also known as the "frequency factor"), *t* represents reaction time, k_B is the Boltzmann constant, *T* is the effective temperature, and E_a is the activation energy (equation 1).[3,7,9]

$$\ln\left(-\ln\frac{[R]}{[R]+[P]}\right) = lnA + lnt - \frac{E_a}{k_B T} \quad (1)$$

This equation is derived from the Arrhenius equation (equation 2) as well as the formula for the rate constant of pseudo-first order kinetics (equation 3), where $[R]$ represents the abundance of precursor ion, and $[P]$ represents the abundance of product ions detected by the instrument.[7] These quantities can both be determined from CID and CIU plots.

$$k = Ae^{-E_a/k_BT}$$

(2)

$$[R]_t = [R]_0 e^{-kt} = ([R] + [P])e^{-kt}$$

(3)

Two more thermochemical values related to A and E_a that may be obtained from CID and CIU are the transition state enthalpy and transition state entropy, $\Delta H^{\ddagger}$ and $\Delta S^{\ddagger}$, respectively.[7,10] Transition state enthalpy is the net energy released or added to the system upon formation of the transition state, while transition state entropy is, at its core, a measure of the number of ways the transition state structure can be reached.[12] A system with a more "rigid and ordered" transition state configuration will have lower $\Delta S^{\ddagger}$, while a system with a more "floppy" transition state will have a higher $\Delta S^{\ddagger}$.[12] To find these values from CID and CIU, the following equation can be used (equation 4), where h represents Planck's constant.[7]

$$\ln\left(\frac{-ln\frac{[R]}{[R]+[P]}}{T}\right) = -\frac{\Delta H^{\ddagger}}{k_BT} + ln\frac{k_BT}{h} + lnt + \frac{\Delta S^{\ddagger}}{k_B}$$

(4)

Internal energy is defined as the sum of all microscopic energies in a molecule. This includes all vibrational, rotational, and electronic energy of the molecule, as well as the sum of the potential energies of each bond within the molecule. To break a particular bond, the energy put into the molecule must be great enough to overcome the bond energy holding the atoms in that bond

together. However, because all of this energy must coincidentally find itself in this bond at the same time, usually much more energy is required to break a bond on the relatively short timescale of the nIM-MS experiment (a few milliseconds or less), resulting in a so-called "kinetic shift".[3,10] For typical nIM-MS instrumentation capable of CID/CIU experiments, this kinetic shift can be very large.[3,10] For example, the Gibbs free energy barrier to unfold the ground state of a native-like protein ion may be a few tens of kJ/mol (i.e., if the ion were allowed an infinite amount of time to unfold). However, the amount of energy that must be added to the ion to unfold it on the timescale of the CIU experiment may be several tens of thousands of kJ/mol. This presents an additional challenge for determining barrier energies with CID/CIU experiments, where accurate thermochemical values need to be determined from experimental values that are often hundreds to thousands of times larger.[3,10]

Current challenges with the nIM-MS technique

While nIM-MS is a competitively fast technique and offers more detailed structural information, there exist several major challenges in making the technique more widely accessible and usable in the chemical and medical research communities. Firstly, different research laboratories may use different commercially available mass spectrometers, each with the capability to perform nIM-MS, but using different instrument design.[13] This can make it very challenging to compare measurements made by different laboratories or even within the same laboratory on different instruments, as the heating, cooling, and dissociation or unfolding processes in each instrument can vary significantly, even though the underlying thermochemistry is of course the same.[13] Kinetic shifts for each instrument and set of experimental parameters may also differ substantially, making it difficult to determine universal thermochemical values

for dissociation or unfolding of a particular ion. This ultimately presents a challenge for the future implementation of nIM-MS calculations for the medical field. Additionally, the lack of understanding about gas-phase statistical mechanics for biomolecules makes modeling the systems and thermodynamics behind CID and CIU increasingly difficult. This means that the use of nIM-MS, CID, and CIU for drug development is useful, but could still be improved by furthering our understanding of how gas-phase and solution-phase mechanics are related.

Ion Simulations of the Physics of Activation (IonSPA)

To address the issues with cross-instrument comparability and lack of understanding of gas-phase mechanics, an accurate, standardized model of heating, cooling, and ion kinetics ideally needs to be created for nIM-MS experiments. The Prell group has developed Ion Simulations of the Physics of Activation, or "IonSPA", as a step towards that standard model. IonSPA models the thermochemistry and kinetics of a molecule that undergoes multiple collisions within the collision cell of the instrument. To do this, we utilize a modified form of a model of collisions called Impulsive Collision Theory (ICT). In ICT, the collision between a neutral gas molecule and the gas-phase biomolecular ion is imagined to take place at a single site (which we call a "pseudo-atom", though it typically represents several nearby atoms) at the surface of the ion.[14] This results in a change in the kinetic energy of the pseudo-atom. As vibrational energy is exchanged between the pseudo-atom and the other atoms in the ion, a new vibrational temperature is established within the ion.[14] Critically, IonSPA improves on the original ICT by also including the possibility to transfer vibrational energy from the pseudo-atom back to the gas particle as it leaves the collision, an essential addition that makes it possible for the ion to cool off once it has been slowed by many collisions and reached its maximum

temperature. This model enables IonSPA to focus on the single point of collisional impact and derive any further energy transfers within the biomolecular ion outside of the singular collision, reducing computation time relative to other much more time-consuming methods, such as atomistic molecular dynamics simulations. To address the issue with commercial instrument cross-comparability, models of the collision region in two widely available commercial instruments, the Waters G2-S*i* and Agilent 6545XT, are programmed for use in IonSPA, allowing for direct comparison of any spectra and thermodynamic behaviors within the program. Based on the ICT model, IonSPA currently is able to determine enthalpy and entropy values for dissociation or unfolding of ions from user-input collisional cross-section values, and full sets of experimental CID/CIU data. The overall goal of this program is to aid in understanding how the gas-phase nature of nIM-MS affects the thermodynamic and kinetic properties of any sample ions and their unfolding patterns, and how those trends may relate to solution-phase mechanics. Additionally, the ability to address the cross-comparability issues between instruments will aid nIM-MS in becoming a far more accurate and robust technique and allow it to be more readily implemented in the medical field in the future.

Vibrational heat capacity and statistical mechanics

To ensure that IonSPA is as accurate as possible, it is essential that the reference data it calls on are accurate and precise. Two of the basic types of input data that ultimately determine the accuracy of collision modeling in IonSPA are the mass of the pseudo-atom and the vibrational heat capacity of the ion. Heat capacity is classically defined as the amount of energy necessary to raise the temperature of one mole of a substance by one Kelvin and, for ions in CID/CIU, is directly related to how the vibrational modes are excited during collisions within a collision cell.[15] Heat capacity at constant pressure, C_p, is a combination of individual heat

capacities for each of the types of energy found in a molecule: translational, rotational, vibrational (harmonic and anharmonic), and electronic.[15] Because the collisions simulated in IonSPA involve vibrational energy exchange, we will concern ourselves primarily with the vibrational heat capacity at constant pressure. (For large protein-sized ions at realistic temperatures, rotational energy constitutes only a very small fraction of the internal energy as compared to vibrational energy.) The formula for vibrational heat capacity can be derived directly from the equations for the vibrational canonical ensemble partition function (Q) and the Helmholtz free energy (A).[15] Equation 5 shows the canonical ensemble partition function, where N represents the number of particles in the system, β represents the quantity $\frac{1}{k_B T}$ (the reciprocal of the Boltzmann constant multiplied by temperature), ω is the angular frequency of a particular vibration, and $\hbar$ is Planck's constant divided by 2π.[15] Equation 6 shows the equation for Helmholtz free energy in the canonical ensemble, using the result from equation 5 as Q.[15] Note that the zero-point energy $\frac{1}{2}N\hbar\omega$ should be excluded from the heat capacity formula as it has no dependence on the beta term and will go away upon taking the derivative.[15] By combining these equations according to equation 7, we obtain the formula for vibrational heat capacity with constant volume for the canonical ensemble.[15]

$$Q = \prod_{\omega} \frac{e^{-\frac{1}{2}N\hbar\omega\beta}}{N!} \left(\frac{1}{1 - e^{-\hbar\omega\beta}}\right)^N$$

(5)

$$A = \frac{-lnQ}{\beta} = \sum_{\omega} \frac{1}{2} N\hbar\omega + \frac{lnN!}{\beta} + \frac{N}{\beta} \ln\left(1 + e^{-\hbar\omega\beta}\right)$$

(6)

$$C_{v,vib} = -2k_B\beta^2\left(\frac{\partial A}{\partial \beta}\right) + k_B\beta^3\left(\frac{\partial^2 A}{\partial \beta^2}\right) = \sum_{\omega}\frac{k_B N\beta^2(\hbar\omega)^2}{(1-e^{\hbar\omega\beta})^2}$$

(7)

Generally, heat capacities of gas-phase ions are very difficult to measure directly, and modeling them accurately requires the use of highly computationally expensive quantum mechanical modeling. However, it is known that the vibrational heat capacities of dry protein powders, for example, vary only slightly from protein to protein.[16,17] This can be explained rather straightforwardly based on the fact that proteins are all built almost entirely from the same set of twenty amino acids and have approximately the same mole ratios of their constituent atoms (hydrogen, carbon, oxygen, nitrogen, phosphorus, and sulfur, primarily). Because the types of chemical bonds and larger-scale structural features are similar across virtually all proteins, the distribution of their vibrational normal mode frequencies and reduced masses is nearly uniform across all proteins. (A similar argument can be made for DNA and RNA.) Thus, we hypothesized that the vibrational heat capacity of protein and peptide ions, normalized by the total number of atoms in the ion, should be nearly uniform across all proteins, and that a similar rule should hold for other classes of structurally related biomolecular ions (DNA, RNA, lipids, sugars, and metabolites). To evaluate whether this hypothesis is correct, we used state-of-the-art *ab initio* (i.e., quantum mechanical) modeling for representative ions from each of these biomolecule classes.

Methods

Initial ion structures for prototypical lipids, short peptides and oligonucleotides, small-molecule drugs, sugars, and 3 of the Agilent Tune Mix (cyclotriphosphazene-based) series were modeled in Avogadro software using its built-in Universal Force Field (UFF) and exported for further geometry optimization and harmonic frequency computations in Gaussian v.09. To determine dependence of computed vibrational heat capacity curves on level of theory and basis set, harmonic frequencies were calculated for the geometry-optimized (protonated) Agilent Tune Mix 322 (2,2,4,4,6,6-hexamethoxycyclotriphosphazene) ion (structure in Fig. 3) using B3LYP/6-31G(d), B3LYP/6-31G(d,p), B3LYP/6-31+G(d,p), and M06-2X/6-31G(d) levels of theory. Vibrational heat capacities were computed from the resulting harmonic frequencies using a statistical mechanics-based Perl script (thermo.pl) developed by the NIST Chemical Informatics Group, which was slightly modified to exclude rotational and electronic heat capacity contributions.[18] Computed vibrational heat capacity values were then normalized per degree of vibrational freedom (i.e., by a factor of $3N-6$, with N the total number of atoms), to facilitate comparison of results across molecules and classes.

All additional species were studied using the B3LYP/6-31G(d) level of theory for final geometry optimization and vibrational frequency calculations but an otherwise identical protocol to the Agilent Tune Mix ions described above. Lipids modeled included palmitoyl-oleoyl-phosphatidic acid (POPA), palmitoyl-oleoyl-phosphatidylcholine (POPC), cholesterol, tetraoleoylcardiolipin, and teristearyltriglyceride (a glycolipid). Oligonucleotides modeled included all 4 DNA nucleotides, as well as uracil nucleotide, and a single strand of both GCGC and ATAT helix. Small-molecule drugs tested include verapamil, ondansetron, acetaminophen, and clozapine N-oxide. Sugars tested were D-glucose and sucrose. All 20 common amino acids

were investigated, and modeled proteins included poly-L-alanine with chain lengths 2, 5, and 10, as well as polyglutamic acid with chain lengths 2, 5, and 10. Effects of secondary structure were also examined using penta-L-alanine and penta-L-tyrosine in both alpha-helix and straight-chain conformations. Because the aim of this study is to study vibrational heat capacity for individual structures as a function of temperature, unfolding, dissociation, and other structural rearrangements were not investigated.

Ion internal energy as a function of time is simulated using a home-built program, Ion Simulations of the Physics of Activation ("IonSPA"), based on the Impulsive Collision Model of Uggerud and Derrick to which a number of key features have been added.[14] These include Monte Carlo simulation of gas-ion collisions within an experimentally realistic electric field and gas pressure, inclusion of superelastic collisions (which are needed for the ion to lose internal energy, i.e. cool off, in some collisions), and tracking of ion kinetic energy as it moves through the collisional activation region. Internal energy distributions as a function of time are compared to Boltzmann distributions with the same mean internal energy using the Beyer-Swinehart density of states algorithm and computed harmonic vibrational frequencies for the ion of interest.[19]

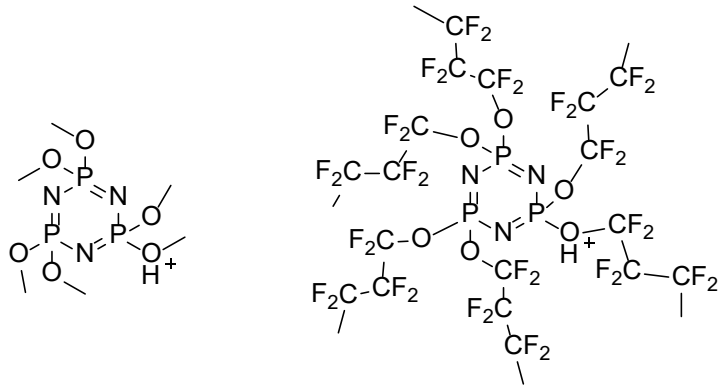

Agilent Tune Mix 322 ion Agilent Tune Mix 1222 ion

Figure 3: Singly protonated (cyclotriphosphazene-based) Agilent Tune Mix 322 and 1222 ion structures.

Results

Choice of ion classes and example structures

Role of heavy atoms in ion sample choice

We expect that the presence of "heavy atoms", here meaning any atoms heavier than oxygen, typically fluorine and phosphorus, will have the greatest effect on vibrational heat capacity. This is because modes that include multiple heavy atoms are the only modes with low-energy vibrational frequencies (i.e., corresponding to energies below k_BT). These are then the only modes that will be significantly excited at temperatures of 200-3000 K, a temperature range that should span the vibrational temperatures encountered in the vast majority of CID/CIU experiments on biomolecules and small drug-like molecules. It was observed early in our studies that vibrational heat capacities varied greatly between classes of ions with and without these heavy atoms, and that those classes with high mole fractions of hydrogen atoms naturally grouped. SI Table 1 shows the mole fraction of hydrogen for each compound we considered for this study, and average mole fraction of hydrogen values for each class of biomolecule is listed in Table 1. Therefore, to limit our computational expense, we chose to examine those compounds that fell at the extremes of their class in terms of heavy atom and hydrogen mole fraction. All other compounds within these classes are then expected to lie within the two extremes.

Eyring Rate Theory for computing protein transition kinetics

IonSPA makes use of Eyring Rate Theory, rather than the more accurate but significantly more computationally expensive RRKM theory to calculate transition kinetics. RRKM, or Rice-Rampsberger-Kassel-Marcus theory requires exact density of states information and accurate

calculation of all oscillator transition strengths and frequencies.[20,21] Due to the sheer overwhelming number of calculations necessary to calculate RRKM rate constant for a large protein-sized ion, estimated as the number of atoms raised to the third power, it is not currently a suitable method for proteins.[20] Arrhenius kinetics are another alternative kinetic model, but are less preferable due to their empirical nature, rather than the first principles based model of Eyring rate theory.[22] Arrhenius kinetic equations also use a constant, A, that is by definition temperature independent.[22] While over a short range of temperatures this would be acceptable, proteins heat to very high temperatures during the unfolding process, over which range the Arrhenius approximation is likely invalid.[22] By contrast, the entropy term in the Eyring rate constant expression is explicitly temperature-dependent. These two limitations motivate the use of Eyring rate theory in IonSPA to compute kinetic information about proteins in scenarios that are not well suited to RRKM or Arrhenius kinetics.

General appearance of computed heat capacity curves.

For all classes of ion tested, computed heat capacities per vibrational degree of freedom (dof) (see Fig. 4) have an approximately linear dependence on temperature up to room temperature (~300 K) and subsequently decay asymptotically toward the thermodynamic limit value (8.3145 J/mol·K) at higher temperatures. Unlike typical Debye curves for simple solids, there is no significant range of temperatures near 0 K for which a markedly cubic dependence on temperature is computed. This is attributed to the lack of very low-frequency phonons in these gas phase monomeric ions, which otherwise dominate the heat capacity of many crystalline solids at very low temperature. For the entire range of temperatures investigated, the Agilent

Tune Mix ions have the highest heat capacities per vibrational degree of freedom, followed by oligonucleotides, and differences for the other ions studied are much smaller.

Ion Class	Average Hydrogen Mole Fraction
Peptides:	0.51
Small-molecule Drugs:	0.49
Nucleotides:	0.37
Lipids:	0.61
Agilent Tune Mix:	0.28
Sugars:	0.49

Table 1: Average hydrogen mole fraction for each biomolecular ion class

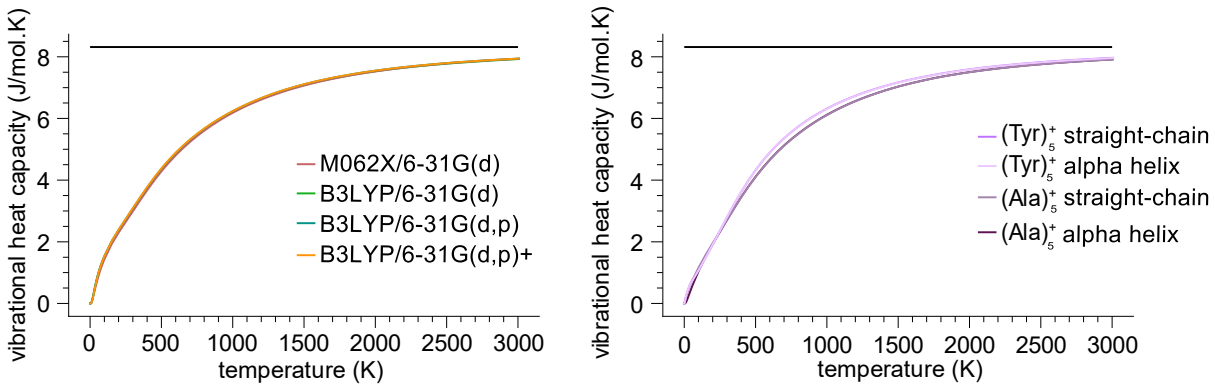

Figure 4. (left) vibrational heat capacity of the Agilent Tune Mix 322 ion using varying levels of theory and basis sets. (right) vibrational heat capacity of penta-L-alanine and penta-L-tyrosine in straight-chain and alpha helix secondary structures.

Computed heat capacity dependence on level of theory and basis set.

The graph on the left half of Figure 4 shows a comparison of heat capacity per vibrational degree of freedom for Agilent Tune Mix 322 ion (chemical structure show in Fig. 3) computed

using the B3LYP and M062X levels of theory and different basis sets. The four heat capacity curves differ by no more than 9.5% at any temperature over the entire range of temperatures studied (0-5000 K). Additionally, for the range of temperatures wherein most vibrational temperatures are found for CID/U experiments, 200-3000K, the four curves differ by at most 3%, with an average difference of 0.045 J/mol·K, indicating a minimal dependence on level of theory and basis set. This insensitivity can be explained by the much larger contributions of relatively low-frequency vibrations involving multiple heavy atoms to the total vibrational heat capacity in comparison to hydrogen-atom stretches, bends, and torsions, for which harmonic frequency calculations are much more sensitive to level of theory and basis set.[23] Due to the very high computational expense of performing similar geometry optimizations and harmonic frequency calculations on much larger ions (such as polypeptides, see below), all additional *ab initio* computations on other ions were thus performed using the least computationally expensive of these levels of theory (B3LYP/6-31G*).

Agilent Tune Mix ions.

The Agilent Tune Mix ions show the most variability within a single class of molecules among those studied (Fig. 5d). The 322 ion curve is far shallower than the other two Tune Mix ions, with the maximum difference between the three curves being 23.9%. The curve for the 1222 ion is much more similar to that of the 2122 ion than the curve for the 322 ion is to that of the 1222 ion, which can be explained by the atomic compositions of the Tune Mix ions (two of which are shown in Fig. 3). Each Tune Mix ion has the same cyclotriphosphazene ring at the center, but the difference in mass between each ion comes from the addition of CF_2 groups to each of the 6 carbon chains. The addition of these "heavy" fluorine atoms causes the heat capacity to greatly increase per degree of freedom. However, as evidenced by the Tune Mix ions,

the relative effect of adding more heavy atoms decreases with total mass over this ion series. The change in slope of the heat capacity curve from the 322 ion to the 1222 ion is more than double that from the 1222 ion to the 2122 ion for all temperatures from 4 K to 3000 K, despite the mass change being the same. This mass dependence of the corresponding vibrational heat capacity curves was the greatest among all classes of ions studied. This theory is further supported by an inquiry into the heat capacity of Metal Organic Frameworks (MOFs) with Mg and Zn centers by Moosavi et al., which shows the same general heat capacity trend upon inclusion of increasingly heavy atoms.[24]

Peptide ions.

Heat capacities were also computed for straight-chain and alpha-helical forms of protonated penta-L-alanine and penta-L-glutamic acid in order to assess dependence of these values on peptide secondary structure and amino acid composition. Very similar results were obtained not only for the different secondary structures but also for the two different amino acid compositions (Fig. 4, right). The heat capacities of the alpha-helical structures predicted at this level of theory are at most 41.4% higher than those for straight-chain structures at 32 K, a difference of only 0.196 J/mol·K. By contrast, within the temperature range of 200-3000 K the expected range for vibrational temperatures in CID/CIU experiments, the maximum difference is only 2.02%, which occurs at 200 K (a difference of 0.026 J/mol·K). Given the extreme consistency between vibrational heat capacity curves for these secondary structure configurations, all peptides were subsequently modeled using a straight-chain secondary structure. Figure 5c shows the vibrational heat capacity curves for all 6 peptide ions. At low temperatures (i.e., ~0-200 K), all curves are fairly similar, but at temperatures of approximately

400 K, the peptides with larger monomer chain lengths show a lower heat capacity than their counterparts with smaller monomer chain lengths. Notably, the difference in vibrational heat capacity between $(Ala)_2^+$ and $(Glu)_2^+$ is larger than that between $(Ala)_5^+$ and $(Glu)_5^+$, which is in turn larger than the difference between $(Ala)_{10}^+$ and $(Glu)_{10}^+$. This suggests that larger peptide chains will deviate less and less in terms of vibrational heat capacity. These results are again attributed to the insensitivity of the statistics of low-frequency, multi-heavy-atom vibrational modes to the presence or absence of hydrogen bonds, which primarily influence higher-frequency modes with low Boltzmann populations over the temperature range studied.[23] These comparisons indicate that differences in peptide secondary structure likely have only a modest effect on heat capacity per degree of freedom in polypeptide and protein ions. Performing *ab initio* geometry optimizations and vibrational frequency computations on protein ions large enough to possess significant tertiary structure is computationally prohibitive with available methods. However, because tertiary structure should primarily affect the statistics of vibrations involving hydrogen bonds (i.e., due to portions of the protein involved in inter-domain hydrogen bonds and salt bridges), tertiary structure should likewise have only a small effect on heat capacity curves.

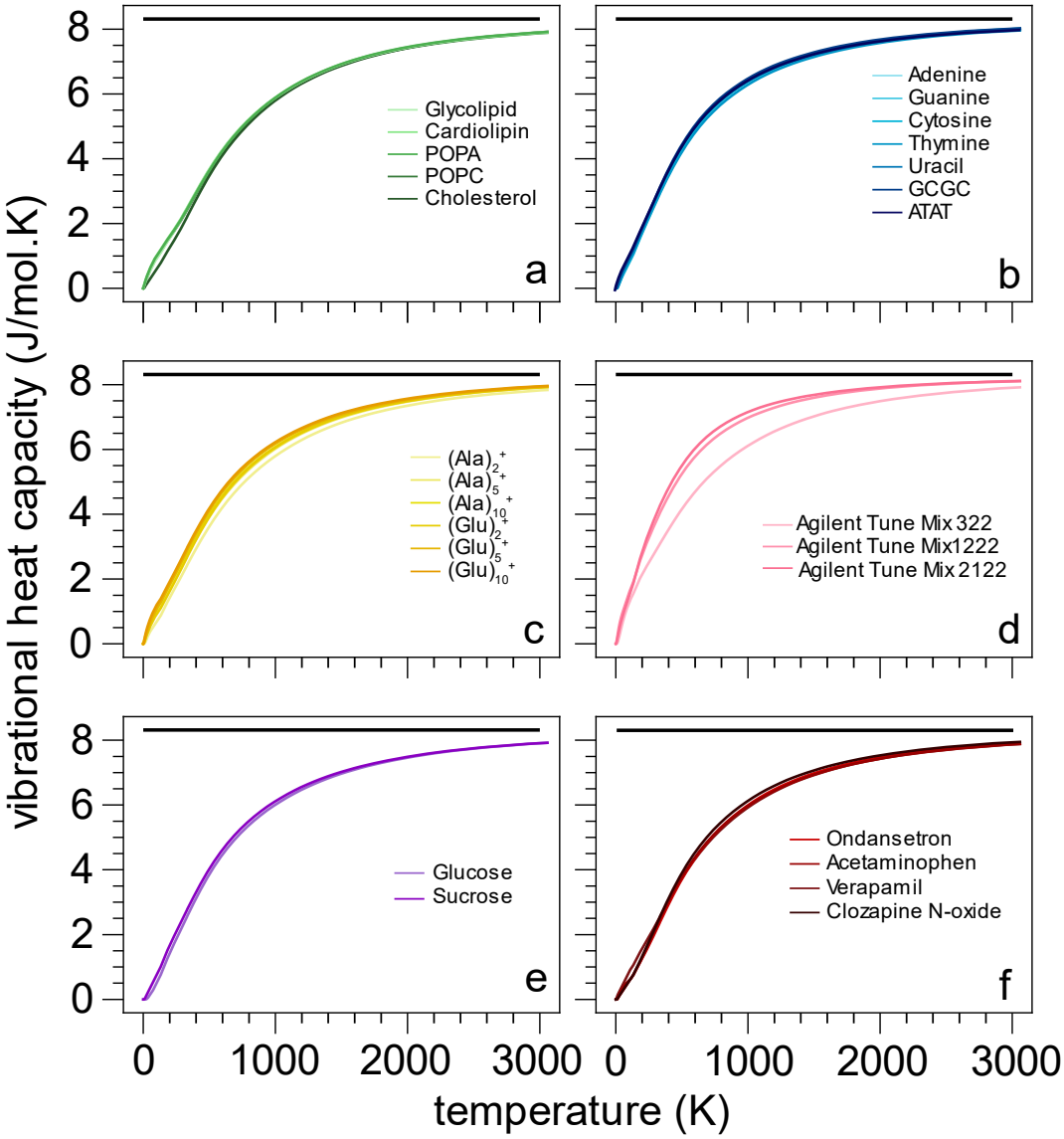

Figure 5. Gas-phase vibrational heat capacities for every biomolecule modeled, separated by biomolecular ion class.

5a: lipid class. 5b: oligonucleotide class. 5c: peptide class. 5d: Agilent Tune Mix class. 5e: sugars class. 5f: small-molecule drugs class.

Lipids.

Lipids span a wide range of chemical structures, from cholesterol-like multi-ring structures to phospholipids and triglycerides. Figure 5 shows the vibrational heat capacity curves per vibrational DOF for each biomolecular ion modeled, separated by class. The lipid class curves are highly consistent, exhibiting significant differences only in the low-temperature region (<500 K) (Fig. 5a). In this range of temperatures, the POPC and cholesterol curves are as much as 31.2% lower than those for the other lipids, but above 500 K, the curves for all five lipids studied are within 4.7% of each other.

(Deoxy)ribonucleotides and oligonucleotides.

Figure 5b shows heat capacities curves computed for all four individual DNA nucleotides and uracil ribonucleotide as well as for single-strand DNA oligonucleotides ATAT and GCGC. (These oligonucleotides were chosen to investigate differences arising from the mole fraction of hydrogen atoms.) These seven heat capacity curves differ by no more than 25% at any temperature, indicating a high degree of similarity across this class of biomolecules. However, the vibrational heat capacity curves for single-strand ATAT (representing smaller nucleobases) and GCGC (representing larger nucleobases) ions separate slightly from those of the single DNA and RNA bases at temperatures above 1000 K, a maximum difference of 2.26% between thymine and the single-strand GCGC.

Small, drug-like organic molecules and sugars.

Small-molecule drugs show a larger difference between curves than most other classes modeled. Computed heat capacity curves for ondansetron and clozapine N-oxide are nearly identical (see Fig. 5f), but acetaminophen has a much higher vibrational heat capacity curve per

degree of freedom, and verapamil has a lower heat capacity curve. Only two sugars were modeled, but trends described above for peptides and oligonucleotides apply to them as well. At a temperature of 1000 K, the vibrational heat capacity curve for sucrose begins to exceed that of glucose, a percent difference of only 1.85%. (Fig. 5e). This can be attributed to the mole ratio of hydrogen for sucrose as compared to glucose. As previously established, a higher hydrogen mole ratio will lead to a shallower vibrational heat capacity curve. Glucose has a hydrogen mole ratio of 0.5, where sucrose has a mole ratio of 0.48. The higher ratio of heavy atoms in sucrose causes additional vibrational modes to be excited, and causes the vibrational heat capacity curve to

approach the thermodynamic limit sooner than that of glucose.

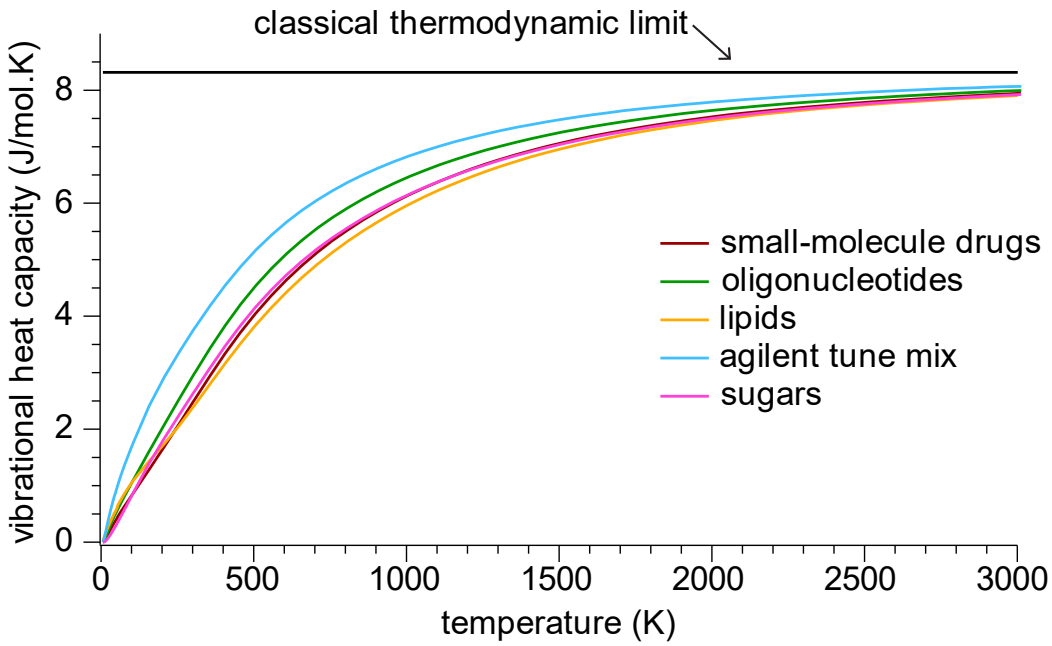

Figure 6. Average vibrational heat capacities per degree of vibrational freedom for small-molecule drugs, peptides, oligonucleotides, Agilent Tune Mix ions, sugars, and lipids.

Comparison of class-average heat capacity curves.

Figure 6 shows the average vibrational heat capacity for each of the 6 biomolecular ion classes. While most classes are similar in their average curves, the Oligonucleotide and Agilent Tune Mix curves are far steeper. This can be explained through the presence of many heavy atoms (phosphorus and fluorine for oligonucleotides and Agilent Tune Mix ions, respectively) not prevalent in the other biomolecular classes, which increases their relative heat capacity. Figure 7 shows the trend for bulk solid proteins in their native state as reported by Gómez et al. in comparison to the trend for gas-phase peptides examined in this study.[16] These results were extrapolated using results for several different protein ions at 298 K, along with a given linear relationship. While results were only given for temperatures under 400 K, the authors report that

this heat capacity trend should be linear for bulk solid proteins near 300 K.[16,17] The small discrepancy between the heat capacity curves computed here and those reported by literature is attributed to the presence of phonon modes in bulk solid data that are absent from gas-phase ions.

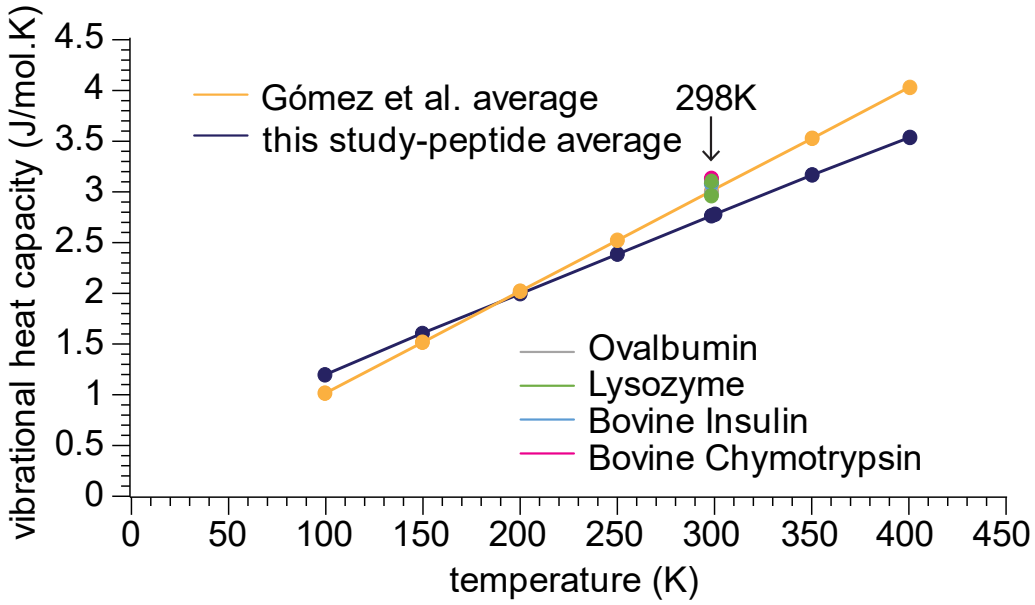

Figure 7. Vibrational heat capacity trends per degree of vibrational freedom for both literature bulk solid proteins and gas-phase peptides.

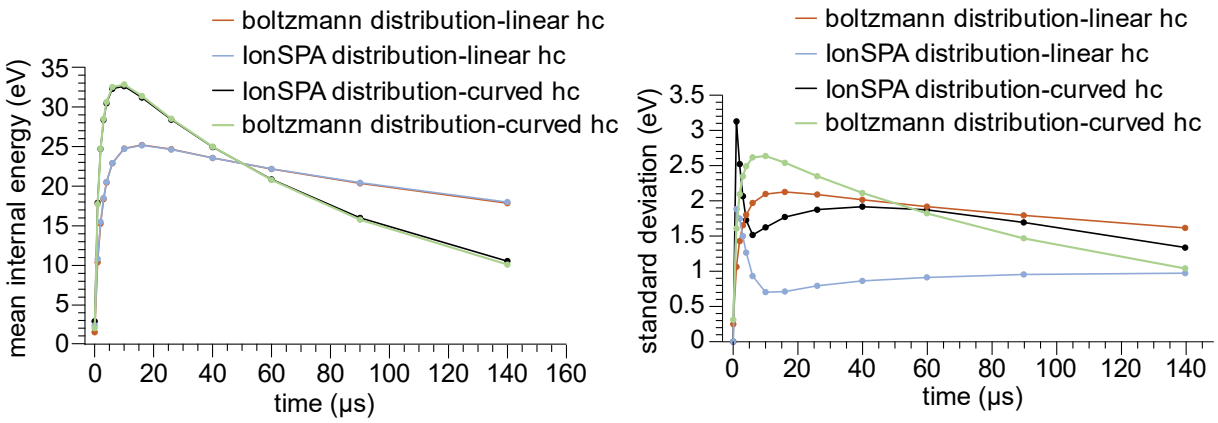

Figure 8. Mean internal energy and standard deviation of IonSPA generated internal energy distributions using a linear heat capacity model and a newly implemented curved heat capacity model.

Effects of heat capacity on modeled ion vibrational energy distributions upon collisional activation.

To understand the thermodynamic nature of the dissociation and unfolding of biomolecules within commercial mass spectrometers, we must have a good grasp on the patterns and fluctuation of any given ion's internal energy as it travels through the instrument. Using internal energy as a figure for comparison in different instrument conditions can provide insight into how those conditions are changing the time scale and manner in which proteins and biomolecules undergo CID or CIU.[9] The inclusion of average heat capacity values computed here for each class of biomolecule causes the widths of each average internal energy peak to show increasing Boltzmann character with increasing time, although there still exists a discrepancy between the widths of these Eyring generated distributions and those of a normal Boltzmann curve at the same temperature (Fig. 8). To understand this discrepancy, it is necessary to investigate the differences in heat capacity and internal energy curves that are generated when the vibrational modes are assumed to be all harmonic, as in the IonSPA code, versus modes of an anharmonic nature. To test this theory, all vibrational modes for $(Ala)_5^+$ and $(Glu)_5^+$ were multiplied by 90% to very roughly account for anharmonicity, the results of which can be found in Figure 9. Based on the ratios of heat capacity values between 100% and 90% vibrational mode values, we can see anharmonicity may increase heat capacity by as much as ~10% within the expected range of vibrational temperatures for large-biomolecule CID/CIU experiments (~200-

1000 K) and by a smaller percentage at higher temperatures. As the temperature increases, however, the ratio of these heat capacities trends towards unity above ~3000 K.

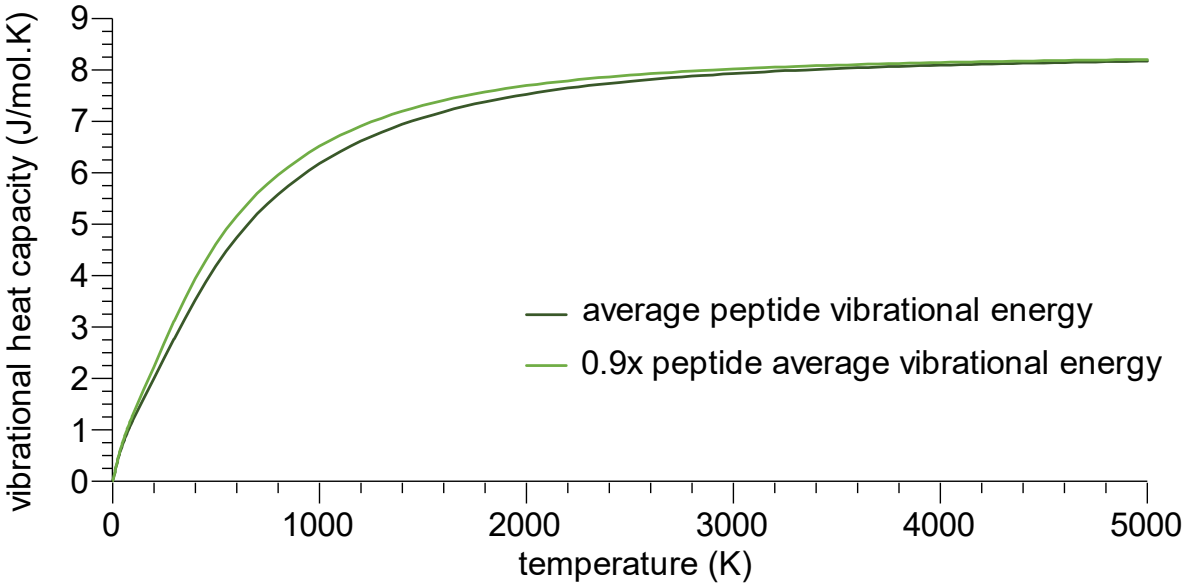

Figure 9. Comparison of peptide vibrational heat capacity average curves with 100% and 90% vibrational modes.

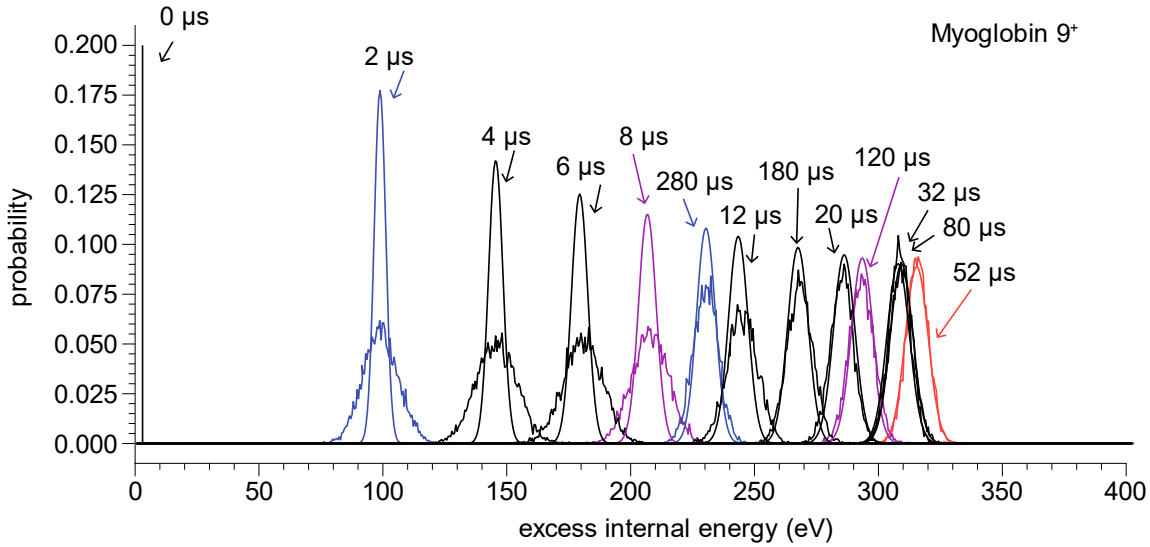

Figure 10. Excess internal energy distribution over time for myoglobin 9+.

Jagged curves represent simulated excess internal energy distributions from IonSPA, and smooth curves represent Boltzmann distributions with the same average internal energy as the simulated distribution for the same time point (and color). Note that all ions were initialized with a delta-distribution of internal energy corresponding to the average energy of a Boltzmann distribution at 298 K.

IonSPA can use Eyring Rate Theory in place of RRKM

High-accuracy, but computationally expensive, RRKM modeling is typically necessary when ion populations do not have a Boltzmann energy distribution, because simpler kinetic models (such as the Arrhenius or Eyring model) require a well-defined internal ion temperature.[20,21] Eyring rate theory, a type of transition state theory, instead requires the involvement of a transition state, defined as a saddle point in the potential energy surface.[14] During the reaction, the population of ions close to the transition state and those of the reactants remain in equilibrium.[25] While it may initially seem unsuited to the reaction process of protein unfolding and dissociation, it is likely that the unfolding of a protein does not occur in a single step, rather a series of steps whose overall kinetics are dominated by a rate-limiting step. The enthalpy and entropy barriers of this rate-limiting step reflect the structural changes required for

the observed dissociation/unfolding event.[25] Based on the results shown in Figure 10 for myoglobin 9, we can see that at higher temperatures, the internal energy distributions begin to take on the shape of a Boltzmann distribution. While the initial internal energy curves during the beginning of the heating process do not show much similarity to their corresponding Boltzmann distributions, it can be assumed that the majority of the reaction will occur at vibrational temperatures within a few percent of the highest temperature.

To ensure that it is acceptable to use Eyring rate theory in place of the more commonly used RRKM rate theory in the IonSPA program, the resulting internal energy distributions must be compared to Boltzmann distributions at the same temperature value.[9,26,27] The full distribution of internal energy curves for the myoglobin 9^+ ion is shown in Figure 10. Upon entering the instrument source, several ions undergo collisions immediately, while some others take far longer to achieve a single collision. This creates a wide internal energy distribution early on that is much broader than a Boltzmann distribution with the same average vibrational energy. However, this distribution rapidly narrows as the ions undergo additional collisions at random times and continue to heat. Once the ions reach their maximum temperature, they begin to cool down and the distribution width begins to increase. Notably, the internal energy distributions are least Boltzmann-like during the first ~20 μs of collisional activation, and become highly Boltzmann-like by the time they reach their maximum temperature (315 K at ~20 μs) and remain Boltzmann-like until they cool by at least 20% on the timescale of ~150 μs. In realistic experiments, the vast majority of dissociation/unfolding contributing to measured CID breakdown curves of CIU fingerprints should occur within this kinetic window, where the protein ions have highly Boltzmann-like distributions.[9,26,27] Upon further cooling, the vibrational distribution becomes slightly wider than a Boltzmann distribution with the same average

vibrational energy. Because Eyring rate theory produces internal energy curves that highly resemble Boltzmann distributions within the kinetic window, IonSPA is able to make use of Eyring theory's faster computation time and lower expense without losing much vital information about the energy of the collision system.

Conclusions

The high consistency between ions in each class of molecule allows us to use the average vibrational heat capacity curve for each class in place of ion-specific curves. In particular, vibrational heat capacity curves for much larger ions (with masses up to many hundreds or even thousands of kDa) for protein and nucleic acid ions, for which ab initio computations are at present impractical, can be readily estimated by multiplying these model curves by the appropriate number of vibrational degrees of freedom (i.e., 3N−6). Implementing the average vibrational heat capacity values for a biomolecular class of ion into IonSPA has been shown here to improve the modeling of internal energies gained by an ion during the full extent of the time it spends undergoing collisions in the collision cell. By proving that IonSPA's internal energy distributions are highly Boltzmann-like within the kinetic window, we have shown that Eyring rate theory is acceptable to use in place of more accurate, but (as of now) computationally intractable, rate theories, like RRKM. The ability to use existing heat capacity values to represent more complex or larger ions whose heat capacities are unable to model allows IonSPA to be far more applicable to CID and CIU analysis and modeling of collisions for many biologically relevant species. Continuing to improve IonSPA's modeling will make it a viable tool for researchers to advance our understanding of unfolding and dissociation events, which we hope will lead to further advancements in drug discovery and treatment in the future.

Supplemental Information

Ion Identity	Hydrogen Mole Fraction
POPC	0.61
POPA	0.61
cholesterol	0.63
tetraoleoylcardiolipin	0.60
arachidonic acid	0.59
tristearyltriglyceride	0.60
“averagine”	0.49
alanine	0.54
arginine	0.54
Asparagine	0.47
aspartic acid	0.44
cysteine	0.5
glutamine	0.5
glutamic acid	0.47
glycine	0.5
histidine	0.45
isoleucine	0.59
leucine	0.59
lysine	0.58
methionine	0.55
phenylalanine	0.48
proline	0.53
serine	0.5
threonine	0.53
tryptophan	0.44
tyrosine	0.46
valine	0.58
$C_nH_{2n}O_n$ (simple sugar)	0.5
sialic acid (neuraminic)	0.49
n-ethylaniline	0.55
acetaminophen	0.45
alprenolol	0.56
ondansetron	0.46
clozapine N-oxide	0.44
colchicine	0.46
verapamil	0.54
reserpine	0.48
adenine (A)	0.37

thymine (T)	0.4
guanine (G)	0.36
cytosine (C)	0.39
uracil	0.36
GCGC	0.36
ATAT	0.37
ATAT/GCGC (double-stranded DNA)	0.36
Agilent Tune Mix 322 ion	0.51
Agilent Tune Mix 1222 ion	0.21
Agilent Tune Mix 2122 ion	0.13

SI Table 1: Hydrogen mole fraction of biomolecules from all classes.

T(K)	POPC	cholesterol	tetraoleoylcardiolipin	teristearyltriglyceride	POPA
0	0.00000	0.00000	0.00000	0.00000	0.00000
2	0.02395	0.00000	0.03382	0.01620	0.03169
4	0.06383	0.00208	0.08420	0.05469	0.07066
6	0.09817	0.01290	0.12350	0.09148	0.10851
8	0.12984	0.03105	0.15894	0.12457	0.14682
10	0.16061	0.05156	0.19403	0.15559	0.18542
12	0.19099	0.07165	0.22887	0.18562	0.22297
14	0.22100	0.09048	0.26300	0.21501	0.25876
16	0.25062	0.10810	0.29615	0.24377	0.29267
18	0.27981	0.12480	0.32828	0.27188	0.32492
20	0.30857	0.14090	0.35947	0.29933	0.35577
22	0.33691	0.15660	0.38981	0.32617	0.38551
24	0.36482	0.17206	0.41942	0.35247	0.41435
26	0.39232	0.18739	0.44839	0.37830	0.44245
28	0.41940	0.20264	0.47678	0.40372	0.46994
30	0.44608	0.21787	0.50465	0.42876	0.49689
32	0.47235	0.23310	0.53201	0.45345	0.52337
34	0.49821	0.24836	0.55888	0.47781	0.54939
36	0.52366	0.26367	0.58526	0.50183	0.57497
38	0.54869	0.27904	0.61117	0.52551	0.60013
40	0.57329	0.29447	0.63658	0.54884	0.62485
42	0.59746	0.30998	0.66151	0.57182	0.64914
44	0.62121	0.32556	0.68593	0.59445	0.67299
46	0.64451	0.34122	0.70987	0.61673	0.69638
48	0.66739	0.35696	0.73331	0.63865	0.71933
50	0.68983	0.37277	0.75625	0.66021	0.74183

52	0.71185	0.38864	0.77871	0.68142	0.76388
54	0.73345	0.40458	0.80069	0.70230	0.78547
56	0.75463	0.42057	0.82219	0.72284	0.80663
58	0.77542	0.43660	0.84323	0.74305	0.82734
60	0.79580	0.45267	0.86382	0.76294	0.84762
62	0.81580	0.46877	0.88398	0.78252	0.86749
64	0.83543	0.48488	0.90371	0.80181	0.88694
66	0.85470	0.50100	0.92302	0.82081	0.90599
68	0.87362	0.51712	0.94195	0.83954	0.92465
70	0.89220	0.53323	0.96048	0.85799	0.94295
72	0.91045	0.54932	0.97865	0.87619	0.96088
74	0.92839	0.56538	0.99647	0.89414	0.97846
76	0.94602	0.58141	1.01394	0.91184	0.99570
78	0.96336	0.59740	1.03109	0.92932	1.01263
80	0.98043	0.61333	1.04793	0.94657	1.02925
82	0.99722	0.62921	1.06447	0.96360	1.04557
84	1.01375	0.64503	1.08072	0.98043	1.06161
86	1.03004	0.66079	1.09670	0.99705	1.07737
88	1.04608	0.67648	1.11241	1.01348	1.09288
90	1.06189	0.69209	1.12788	1.02971	1.10814
92	1.07748	0.70762	1.14310	1.04577	1.12316
94	1.09286	0.72308	1.15810	1.06164	1.13796
96	1.10804	0.73845	1.17288	1.07734	1.15254
98	1.12302	0.75374	1.18746	1.09288	1.16692
100	1.13781	0.76894	1.20183	1.10825	1.18110
150	1.46574	1.12431	1.52011	1.45404	1.49522
200	1.76661	1.46209	1.81814	1.77125	1.78958
250	2.08742	1.81969	2.14170	2.10504	2.10953
298.15	2.42336	2.18822	2.48207	2.45087	2.44704
300	2.43666	2.20270	2.49555	2.46450	2.46042
350	2.80101	2.59642	2.86412	2.83661	2.82711
400	3.16303	2.98310	3.22915	3.20409	3.19131
450	3.50976	3.35013	3.57760	3.55426	3.53982
500	3.83429	3.69120	3.90275	3.88051	3.86566
550	4.13424	4.00463	4.20250	4.18084	4.16654
600	4.40998	4.29144	4.47743	4.45592	4.44288
650	4.66316	4.55380	4.72935	4.70766	4.69638
700	4.89584	4.79419	4.96044	4.93838	4.92913
750	5.11005	5.01501	5.17284	5.15028	5.14322
800	5.30764	5.21836	5.36848	5.34539	5.34053
850	5.49024	5.40604	5.54900	5.52541	5.52268

900	5.65922	5.57958	5.71586	5.69183	5.69110
950	5.81579	5.74029	5.87028	5.84590	5.84700
1000	5.96101	5.88929	6.01334	5.98872	5.99146
1050	6.09578	6.02757	6.14600	6.12123	6.12544
1100	6.22095	6.15600	6.26909	6.24429	6.24976
1150	6.33728	6.27538	6.38340	6.35866	6.36521
1200	6.44545	6.38640	6.48961	6.46502	6.47249
1250	6.54609	6.48973	6.58836	6.56400	6.57224
1300	6.63978	6.58596	6.68024	6.65618	6.66504
1350	6.72707	6.67563	6.76579	6.74208	6.75144
1400	6.80844	6.75925	6.84549	6.82219	6.83194
1450	6.88434	6.83728	6.91981	6.89694	6.90700
1500	6.95520	6.91015	6.98916	6.96676	6.97703
1550	7.02140	6.97826	7.05393	7.03202	7.04243
1600	7.08330	7.04196	7.11446	7.09306	7.10356
1650	7.14122	7.10160	7.17109	7.15021	7.16074
1700	7.19547	7.15746	7.22411	7.20375	7.21427
1750	7.24632	7.20984	7.27379	7.25396	7.26443
1800	7.29403	7.25900	7.32039	7.30108	7.31148
1850	7.33882	7.30517	7.36413	7.34535	7.35563
1900	7.38092	7.34857	7.40523	7.38696	7.39712
1950	7.42051	7.38940	7.44387	7.42611	7.43614
2000	7.45779	7.42785	7.48025	7.46299	7.47285
2050	7.49290	7.46409	7.51452	7.49774	7.50744
2100	7.52602	7.49827	7.54683	7.53052	7.54005
2150	7.55728	7.53054	7.57731	7.56147	7.57082
2200	7.58680	7.56102	7.60611	7.59072	7.59988
2250	7.61471	7.58984	7.63332	7.61837	7.62735
2300	7.64112	7.61712	7.65907	7.64453	7.65333
2350	7.66612	7.64295	7.68344	7.66932	7.67793
2400	7.68982	7.66743	7.70653	7.69281	7.70123
2450	7.71229	7.69065	7.72843	7.71510	7.72333
2500	7.73361	7.71269	7.74921	7.73625	7.74430
2550	7.75386	7.73363	7.76895	7.75635	7.76421
2600	7.77311	7.75353	7.78770	7.77545	7.78313
2650	7.79142	7.77246	7.80554	7.79362	7.80113
2700	7.80884	7.79048	7.82251	7.81092	7.81826
2750	7.82544	7.80765	7.83868	7.82740	7.83457
2800	7.84126	7.82401	7.85408	7.84311	7.85011
2850	7.85634	7.83961	7.86877	7.85810	7.86493
2900	7.87073	7.85451	7.88279	7.87240	7.87908

2950	7.88448	7.86873	7.89618	7.88606	7.89258
3000	7.89761	7.88232	7.90896	7.89911	7.90548
3050	7.91017	7.89532	7.92119	7.91159	7.91781
3100	7.92218	7.90775	7.93288	7.92353	7.92961
3150	7.93368	7.91966	7.94408	7.93496	7.94090
3200	7.94469	7.93105	7.95480	7.94591	7.95172
3250	7.95524	7.94198	7.96507	7.95640	7.96208
3300	7.96535	7.95245	7.97491	7.96647	7.97201
3350	7.97506	7.96250	7.98436	7.97612	7.98154
3400	7.98437	7.97215	7.99342	7.98538	7.99068
3450	7.99331	7.98141	8.00212	7.99428	7.99946
3500	8.00190	7.99030	8.01049	8.00283	8.00789
3550	8.01016	7.99886	8.01852	8.01105	8.01600
3600	8.01810	8.00709	8.02625	8.01895	8.02380
3650	8.02574	8.01500	8.03368	8.02655	8.03130
3700	8.03309	8.02262	8.04084	8.03387	8.03851
3750	8.04018	8.02995	8.04773	8.04092	8.04546
3800	8.04699	8.03702	8.05437	8.04771	8.05216
3850	8.05357	8.04383	8.06076	8.05426	8.05861
3900	8.05991	8.05040	8.06693	8.06057	8.06483
3950	8.06602	8.05674	8.07288	8.06666	8.07083
4000	8.07192	8.06285	8.07862	8.07253	8.07662
4050	8.07761	8.06875	8.08416	8.07820	8.08221
4100	8.08312	8.07445	8.08951	8.08368	8.08760
4150	8.08843	8.07996	8.09468	8.08898	8.09282
4200	8.09356	8.08528	8.09967	8.09409	8.09785
4250	8.09853	8.09042	8.10450	8.09903	8.10273
4300	8.10333	8.09540	8.10917	8.10382	8.10743
4350	8.10797	8.10021	8.11369	8.10845	8.11199
4400	8.11246	8.10488	8.11806	8.11292	8.11640
4450	8.11681	8.10939	8.12229	8.11726	8.12067
4500	8.12103	8.11376	8.12639	8.12146	8.12480
4550	8.12511	8.11799	8.13036	8.12553	8.12881
4600	8.12907	8.12209	8.13421	8.12947	8.13269
4650	8.13290	8.12607	8.13794	8.13329	8.13645
4700	8.13662	8.12992	8.14155	8.13700	8.14010
4750	8.14023	8.13366	8.14506	8.14059	8.14363
4800	8.14372	8.13729	8.14846	8.14408	8.14707
4850	8.14712	8.14081	8.15177	8.14747	8.15040
4900	8.15042	8.14423	8.15497	8.15075	8.15363
4950	8.15362	8.14755	8.15809	8.15394	8.15677

5000	8.15673	8.15077	8.16111	8.15704	8.15982

SI Table 2: Vibrational heat capacity values for all lipids 0-5000K

T(K)	cytosine	uracil	guanine	thymine	adenine	GCGC	ATAT
0	0.00000	0.00000	0.00000	0.00000	0.00000	0.00000	0.00000
2	0.00000	0.00000	0.00000	0.00000	0.00000	0.01493	0.02983
4	0.00041	0.00017	0.00053	0.00004	0.00023	0.05430	0.09258
6	0.00557	0.00366	0.00600	0.00162	0.00367	0.08814	0.13850
8	0.01930	0.01624	0.01860	0.00886	0.01314	0.12065	0.17515
10	0.04060	0.03898	0.03642	0.02355	0.02790	0.15350	0.20942
12	0.06716	0.06918	0.05783	0.04437	0.04673	0.18671	0.24316
14	0.09685	0.10355	0.08175	0.06932	0.06869	0.21983	0.27647
16	0.12805	0.13952	0.10736	0.09676	0.09293	0.25242	0.30912
18	0.15965	0.17538	0.13399	0.12556	0.11871	0.28423	0.34088
20	0.19094	0.21016	0.16109	0.15494	0.14532	0.31513	0.37165
22	0.22153	0.24347	0.18824	0.18442	0.17224	0.34509	0.40142
24	0.25118	0.27520	0.21513	0.21368	0.19906	0.37415	0.43021
26	0.27984	0.30545	0.24160	0.24253	0.22549	0.40236	0.45810
28	0.30747	0.33442	0.26754	0.27084	0.25138	0.42979	0.48517
30	0.33413	0.36231	0.29293	0.29858	0.27664	0.45652	0.51150
32	0.35987	0.38931	0.31777	0.32573	0.30123	0.48264	0.53719
34	0.38478	0.41561	0.34211	0.35231	0.32519	0.50820	0.56229
36	0.40896	0.44133	0.36598	0.37836	0.34856	0.53327	0.58689
38	0.43246	0.46658	0.38945	0.40391	0.37138	0.55791	0.61104
40	0.45539	0.49143	0.41257	0.42901	0.39376	0.58215	0.63479
42	0.47780	0.51596	0.43537	0.45370	0.41574	0.60604	0.65819
44	0.49975	0.54017	0.45793	0.47803	0.43738	0.62961	0.68127
46	0.52133	0.56413	0.48025	0.50203	0.45876	0.65288	0.70406
48	0.54257	0.58783	0.50240	0.52575	0.47991	0.67588	0.72659
50	0.56354	0.61129	0.52438	0.54921	0.50087	0.69863	0.74890
52	0.58426	0.63454	0.54624	0.57245	0.52169	0.72114	0.77098
54	0.60478	0.65757	0.56798	0.59549	0.54239	0.74343	0.79287
56	0.62514	0.68039	0.58963	0.61836	0.56301	0.76551	0.81458
58	0.64535	0.70302	0.61121	0.64107	0.58356	0.78740	0.83611
60	0.66546	0.72546	0.63273	0.66365	0.60404	0.80911	0.85749
62	0.68548	0.74772	0.65419	0.68609	0.62448	0.83065	0.87871
64	0.70544	0.76982	0.67561	0.70842	0.64489	0.85202	0.89979
66	0.72534	0.79175	0.69699	0.73065	0.66526	0.87325	0.92073
68	0.74522	0.81353	0.71834	0.75279	0.68562	0.89434	0.94155
70	0.76505	0.83517	0.73968	0.77483	0.70594	0.91529	0.96224

72	0.78488	0.85667	0.76098	0.79679	0.72625	0.93612	0.98282
74	0.80471	0.87804	0.78226	0.81867	0.74655	0.95683	1.00328
76	0.82454	0.89930	0.80352	0.84046	0.76682	0.97743	1.02363
78	0.84437	0.92045	0.82476	0.86218	0.78707	0.99793	1.04387
80	0.86420	0.94149	0.84598	0.88383	0.80731	1.01833	1.06402
82	0.88406	0.96244	0.86718	0.90540	0.82753	1.03864	1.08407
84	0.90392	0.98330	0.88834	0.92690	0.84773	1.05886	1.10402
86	0.92381	1.00406	0.90949	0.94831	0.86791	1.07901	1.12388
88	0.94369	1.02475	0.93061	0.96966	0.88806	1.09908	1.14366
90	0.96359	1.04538	0.95170	0.99093	0.90819	1.11907	1.16335
92	0.98352	1.06591	0.97276	1.01211	0.92830	1.13900	1.18296
94	1.00344	1.08640	0.99378	1.03322	0.94839	1.15886	1.20249
96	1.02337	1.10681	1.01478	1.05426	0.96845	1.17867	1.22194
98	1.04330	1.12716	1.03575	1.07521	0.98848	1.19841	1.24132
100	1.06325	1.14746	1.05667	1.09608	1.00849	1.21810	1.26063
150	1.55715	1.64230	1.56631	1.59249	1.49948	1.69856	1.72681
200	2.03699	2.12338	2.05568	2.05518	1.97731	2.16909	2.17863
250	2.50795	2.59712	2.53380	2.50549	2.44942	2.63662	2.62880
298.15	2.95085	3.04217	2.98164	2.93084	2.89610	3.07859	3.05789
300	2.96754	3.05892	2.99849	2.94693	2.91298	3.09526	3.07415
350	3.40534	3.49799	3.44032	3.37107	3.35726	3.53324	3.50320
400	3.81155	3.90465	3.85023	3.76819	3.77168	3.94023	3.90487
450	4.18082	4.27374	4.22310	4.13224	4.14996	4.31061	4.27257
500	4.51225	4.60451	4.55796	4.46146	4.49039	4.64322	4.60435
550	4.80790	4.89908	4.85674	4.75712	4.79453	4.93991	4.90145
600	5.07133	5.16102	5.12278	5.02206	5.06557	5.20404	5.16681
650	5.30652	5.39438	5.36002	5.25976	5.30737	5.43947	5.40399
700	5.51727	5.60299	5.57224	5.47363	5.52376	5.64996	5.61655
750	5.70700	5.79033	5.76284	5.66679	5.71815	5.83890	5.80770
800	5.87860	5.95937	5.93480	5.84194	5.89355	6.00920	5.98027
850	6.03451	6.11255	6.09060	6.00134	6.05246	6.16333	6.13665
900	6.17671	6.25195	6.23232	6.14693	6.19703	6.30336	6.27884
950	6.30688	6.37926	6.36169	6.28028	6.32899	6.43102	6.40854
1000	6.42640	6.49590	6.48016	6.40275	6.44981	6.54773	6.52718
1050	6.53641	6.60308	6.58893	6.51546	6.56073	6.65472	6.63595
1100	6.63790	6.70178	6.68905	6.61943	6.66281	6.75303	6.73590
1150	6.73172	6.79288	6.78140	6.71547	6.75694	6.84356	6.82792
1200	6.81859	6.87711	6.86674	6.80434	6.84391	6.92706	6.91279
1250	6.89914	6.95512	6.94572	6.88670	6.92438	7.00422	6.99119
1300	6.97395	7.02747	7.01894	6.96310	6.99898	7.07563	7.06373
1350	7.04351	7.09468	7.08692	7.03407	7.06821	7.14181	7.13094

1400	7.10825	7.15719	7.15012	7.10008	7.13256	7.20324	7.19328
1450	7.16859	7.21540	7.20893	7.16154	7.19242	7.26032	7.25120
1500	7.22489	7.26967	7.26375	7.21882	7.24820	7.31344	7.30507
1550	7.27746	7.32031	7.31488	7.27227	7.30023	7.36292	7.35523
1600	7.32662	7.36763	7.36264	7.32220	7.34882	7.40907	7.40199
1650	7.37262	7.41189	7.40729	7.36888	7.39422	7.45216	7.44564
1700	7.41571	7.45333	7.44909	7.41258	7.43673	7.49244	7.48643
1750	7.45611	7.49217	7.48825	7.45351	7.47654	7.53014	7.52458
1800	7.49403	7.52861	7.52497	7.49189	7.51386	7.56545	7.56031
1850	7.52965	7.56283	7.55944	7.52793	7.54890	7.59857	7.59381
1900	7.56314	7.59499	7.59184	7.56178	7.58181	7.62965	7.62524
1950	7.59466	7.62525	7.62231	7.59362	7.61277	7.65886	7.65476
2000	7.62434	7.65373	7.65100	7.62359	7.64191	7.68634	7.68252
2050	7.65233	7.68059	7.67804	7.65183	7.66936	7.71221	7.70865
2100	7.67874	7.70592	7.70354	7.67845	7.69525	7.73659	7.73326
2150	7.70369	7.72985	7.72761	7.70359	7.71969	7.75958	7.75647
2200	7.72726	7.75245	7.75034	7.72732	7.74278	7.78128	7.77838
2250	7.74955	7.77383	7.77184	7.74977	7.76461	7.80180	7.79907
2300	7.77066	7.79405	7.79220	7.77101	7.78525	7.82119	7.81864
2350	7.79066	7.81323	7.81147	7.79112	7.80481	7.83955	7.83716
2400	7.80962	7.83140	7.82974	7.81018	7.82335	7.85694	7.85469
2450	7.82761	7.84863	7.84707	7.82825	7.84093	7.87343	7.87131
2500	7.84470	7.86500	7.86352	7.84541	7.85763	7.88908	7.88707
2550	7.86094	7.88056	7.87915	7.86172	7.87347	7.90393	7.90204
2600	7.87637	7.89534	7.89401	7.87720	7.88855	7.91805	7.91626
2650	7.89105	7.90941	7.90815	7.89195	7.90289	7.93147	7.92978
2700	7.90504	7.92281	7.92160	7.90597	7.91654	7.94424	7.94264
2750	7.91838	7.93557	7.93442	7.91933	7.92954	7.95641	7.95489
2800	7.93109	7.94774	7.94665	7.93208	7.94193	7.96800	7.96656
2850	7.94322	7.95935	7.95831	7.94422	7.95376	7.97905	7.97768
2900	7.95480	7.97044	7.96944	7.95583	7.96504	7.98960	7.98829
2950	7.96585	7.98102	7.98008	7.96690	7.97582	7.99966	7.99843
3000	7.97642	7.99115	7.99024	7.97748	7.98612	8.00929	8.00811
3050	7.98654	8.00083	7.99995	7.98761	7.99597	8.01848	8.01736
3100	7.99622	8.01009	8.00925	7.99728	8.00539	8.02728	8.02621
3150	8.00547	8.01896	8.01816	8.00656	8.01441	8.03570	8.03467
3200	8.01435	8.02745	8.02669	8.01543	8.02306	8.04376	8.04278
3250	8.02286	8.03559	8.03485	8.02394	8.03134	8.05149	8.05055
3300	8.03102	8.04340	8.04270	8.03210	8.03928	8.05890	8.05800
3350	8.03885	8.05089	8.05022	8.03993	8.04691	8.06600	8.06514
3400	8.04637	8.05809	8.05743	8.04744	8.05422	8.07282	8.07199

3450	8.05359	8.06500	8.06436	8.05466	8.06125	8.07936	8.07858
3500	8.06053	8.07163	8.07103	8.06159	8.06800	8.08566	8.08490
3550	8.06720	8.07802	8.07743	8.06825	8.07448	8.09170	8.09097
3600	8.07361	8.08416	8.08360	8.07466	8.08073	8.09751	8.09681
3650	8.07980	8.09006	8.08952	8.08083	8.08674	8.10310	8.10243
3700	8.08574	8.09575	8.09523	8.08677	8.09252	8.10849	8.10784
3750	8.09146	8.10124	8.10073	8.09248	8.09808	8.11367	8.11305
3800	8.09698	8.10652	8.10602	8.09799	8.10344	8.11866	8.11806
3850	8.10230	8.11160	8.11113	8.10329	8.10862	8.12348	8.12290
3900	8.10743	8.11651	8.11605	8.10841	8.11361	8.12812	8.12756
3950	8.11238	8.12125	8.12079	8.11335	8.11841	8.13259	8.13205
4000	8.11716	8.12581	8.12538	8.11812	8.12306	8.13691	8.13639
4050	8.12177	8.13023	8.12980	8.12272	8.12754	8.14108	8.14057
4100	8.12623	8.13448	8.13408	8.12716	8.13187	8.14510	8.14462
4150	8.13053	8.13860	8.13821	8.13145	8.13605	8.14899	8.14852
4200	8.13469	8.14258	8.14220	8.13561	8.14009	8.15275	8.15229
4250	8.13871	8.14643	8.14606	8.13962	8.14400	8.15639	8.15594
4300	8.14260	8.15015	8.14978	8.14349	8.14778	8.15990	8.15947
4350	8.14637	8.15375	8.15340	8.14725	8.15143	8.16330	8.16288
4400	8.15001	8.15724	8.15689	8.15088	8.15498	8.16659	8.16619
4450	8.15355	8.16061	8.16028	8.15440	8.15840	8.16977	8.16938
4500	8.15696	8.16388	8.16356	8.15781	8.16173	8.17286	8.17248
4550	8.16027	8.16705	8.16674	8.16111	8.16494	8.17585	8.17548
4600	8.16348	8.17012	8.16981	8.16430	8.16806	8.17874	8.17838
4650	8.16659	8.17310	8.17279	8.16740	8.17108	8.18155	8.18120
4700	8.16961	8.17598	8.17569	8.17041	8.17401	8.18427	8.18393
4750	8.17254	8.17877	8.17850	8.17333	8.17685	8.18691	8.18658
4800	8.17538	8.18149	8.18122	8.17616	8.17961	8.18947	8.18915
4850	8.17814	8.18413	8.18386	8.17891	8.18228	8.19196	8.19164
4900	8.18082	8.18669	8.18643	8.18158	8.18488	8.19437	8.19406
4950	8.18341	8.18918	8.18892	8.18416	8.18740	8.19671	8.19642
5000	8.18594	8.19159	8.19134	8.18668	8.18986	8.19898	8.19870

SI Table 3: Vibrational heat capacity values for all oligonucleotides 0-5000K

T(K)	$(Ala)_2^+$	$(Ala)_5^+$	$(Ala)_{10}^+$	$(Glu)_2^+$	$(Glu)_5^+$	$(Glu)_{10}^+$
0	0.00000	0.00000	0.00000	0.00000	0.00000	0.00000
2	0.00000	0.00219	0.02951	0.00029	0.00559	0.01341
4	0.00035	0.02403	0.07570	0.01388	0.03427	0.06203
6	0.00544	0.05737	0.12235	0.04372	0.06805	0.11703
8	0.01862	0.09481	0.16563	0.07809	0.10488	0.17356

10	0.03715	0.13138	0.20458	0.11270	0.14332	0.22843
12	0.05848	0.16626	0.24050	0.14623	0.18180	0.28016
14	0.08152	0.19995	0.27476	0.17850	0.21961	0.32841
16	0.10580	0.23295	0.30821	0.20975	0.25663	0.37340
18	0.13094	0.26547	0.34124	0.24022	0.29296	0.41558
20	0.15648	0.29753	0.37390	0.27011	0.32870	0.45544
22	0.18203	0.32900	0.40610	0.29951	0.36390	0.49339
24	0.20723	0.35975	0.43768	0.32849	0.39856	0.52976
26	0.23179	0.38966	0.46848	0.35703	0.43263	0.56478
28	0.25556	0.41863	0.49841	0.38511	0.46608	0.59862
30	0.27842	0.44663	0.52738	0.41272	0.49887	0.63141
32	0.30039	0.47365	0.55539	0.43980	0.53096	0.66324
34	0.32148	0.49972	0.58246	0.46634	0.56234	0.69418
36	0.34180	0.52493	0.60864	0.49232	0.59301	0.72428
38	0.36142	0.54933	0.63402	0.51773	0.62296	0.75358
40	0.38045	0.57303	0.65866	0.54255	0.65220	0.78212
42	0.39903	0.59611	0.68267	0.56678	0.68075	0.80993
44	0.41723	0.61865	0.70612	0.59046	0.70862	0.83703
46	0.43515	0.64075	0.72909	0.61359	0.73582	0.86347
48	0.45289	0.66247	0.75166	0.63620	0.76238	0.88924
50	0.47050	0.68386	0.77388	0.65830	0.78833	0.91439
52	0.48805	0.70499	0.79580	0.67993	0.81367	0.93893
54	0.50558	0.72589	0.81747	0.70112	0.83844	0.96289
56	0.52311	0.74661	0.83892	0.72188	0.86265	0.98628
58	0.54067	0.76716	0.86017	0.74226	0.88634	1.00913
60	0.55829	0.78756	0.88125	0.76227	0.90952	1.03147
62	0.57595	0.80785	0.90217	0.78195	0.93222	1.05331
64	0.59370	0.82801	0.92294	0.80130	0.95446	1.07467
66	0.61150	0.84807	0.94357	0.82036	0.97627	1.09560
68	0.62936	0.86802	0.96406	0.83916	0.99766	1.11610
70	0.64729	0.88786	0.98441	0.85769	1.01866	1.13620
72	0.66524	0.90760	1.00462	0.87598	1.03928	1.15592
74	0.68326	0.92724	1.02470	0.89405	1.05957	1.17528
76	0.70129	0.94676	1.04464	0.91191	1.07952	1.19431
78	0.71933	0.96619	1.06444	0.92959	1.09916	1.21303
80	0.73739	0.98549	1.08409	0.94708	1.11851	1.23145
82	0.75545	1.00469	1.10361	0.96439	1.13759	1.24960
84	0.77350	1.02377	1.12298	0.98156	1.15641	1.26751
86	0.79153	1.04273	1.14220	0.99857	1.17500	1.28517
88	0.80953	1.06157	1.16127	1.01544	1.19336	1.30263
90	0.82750	1.08029	1.18020	1.03219	1.21152	1.31988

92	0.84542	1.09888	1.19898	1.04881	1.22948	1.33694
94	0.86332	1.11736	1.21762	1.06532	1.24727	1.35384
96	0.88114	1.13571	1.23611	1.08174	1.26489	1.37059
98	0.89891	1.15394	1.25445	1.09804	1.28236	1.38720
100	0.91662	1.17204	1.27266	1.11426	1.29969	1.40367
150	1.33553	1.59081	1.69025	1.50485	1.70874	1.79727
200	1.72200	1.97329	2.07014	1.89460	2.10705	2.18880
250	2.10152	2.35000	2.44473	2.29545	2.50923	2.58743
298.15	2.46879	2.71481	2.80767	2.68662	2.89739	2.97291
300	2.48289	2.72881	2.82159	2.70161	2.91221	2.98763
350	2.86071	3.10345	3.19418	3.10079	3.30582	3.37858
400	3.22538	3.46399	3.55249	3.48134	3.67960	3.74968
450	3.56921	3.80285	3.88892	3.83567	4.02661	4.09397
500	3.88824	4.11622	4.19973	4.16058	4.34400	4.40861
550	4.18161	4.40342	4.48425	4.45609	4.63198	4.69381
600	4.45035	4.66566	4.74374	4.72405	4.89248	4.95155
650	4.69647	4.90503	4.98032	4.96710	5.12820	5.18452
700	4.92221	5.12387	5.19637	5.18803	5.34195	5.39558
750	5.12977	5.32444	5.39415	5.38946	5.53638	5.58736
800	5.32111	5.50876	5.57570	5.57368	5.71380	5.76222
850	5.49788	5.67854	5.74276	5.74267	5.87622	5.92216
900	5.66155	5.83528	5.89684	5.89810	6.02531	6.06887
950	5.81333	5.98025	6.03921	6.04139	6.16251	6.20379
1000	5.95430	6.11453	6.17096	6.17375	6.28903	6.32814
1050	6.08535	6.23907	6.29307	6.29621	6.40591	6.44297
1100	6.20730	6.35469	6.40634	6.40967	6.51406	6.54917
1150	6.32088	6.46215	6.51154	6.51492	6.61427	6.64754
1200	6.42673	6.56210	6.60933	6.61267	6.70723	6.73878
1250	6.52544	6.65513	6.70030	6.70354	6.79357	6.82349
1300	6.61755	6.74180	6.78500	6.78810	6.87385	6.90223
1350	6.70356	6.82260	6.86392	6.86686	6.94856	6.97550
1400	6.78392	6.89799	6.93752	6.94028	7.01815	7.04376
1450	6.85908	6.96838	7.00621	7.00879	7.08306	7.10739
1500	6.92938	7.03416	7.07037	7.07276	7.14363	7.16678
1550	6.99521	7.09567	7.13035	7.13257	7.20022	7.22226
1600	7.05688	7.15324	7.18647	7.18851	7.25314	7.27413
1650	7.11471	7.20717	7.23901	7.24089	7.30267	7.32268
1700	7.16898	7.25772	7.28826	7.28998	7.34907	7.36816
1750	7.21994	7.30516	7.33445	7.33603	7.39257	7.41080
1800	7.26783	7.34970	7.37781	7.37925	7.43340	7.45082
1850	7.31288	7.39156	7.41856	7.41987	7.47176	7.48841

1900	7.35529	7.43093	7.45687	7.45807	7.50781	7.52376
1950	7.39523	7.46799	7.49293	7.49402	7.54175	7.55701
2000	7.43288	7.50291	7.52690	7.52789	7.57371	7.58834
2050	7.46841	7.53584	7.55892	7.55982	7.60383	7.61786
2100	7.50197	7.56692	7.58914	7.58995	7.63226	7.64572
2150	7.53367	7.59626	7.61767	7.61841	7.65909	7.67202
2200	7.56365	7.62401	7.64463	7.64530	7.68446	7.69687
2250	7.59203	7.65025	7.67014	7.67075	7.70844	7.72038
2300	7.61889	7.67510	7.69428	7.69482	7.73114	7.74264
2350	7.64438	7.69863	7.71715	7.71765	7.75265	7.76372
2400	7.66853	7.72096	7.73884	7.73927	7.77304	7.78370
2450	7.69147	7.74213	7.75941	7.75980	7.79239	7.80266
2500	7.71326	7.76224	7.77894	7.77929	7.81075	7.82066
2550	7.73397	7.78135	7.79750	7.79781	7.82820	7.83776
2600	7.75367	7.79952	7.81514	7.81542	7.84479	7.85402
2650	7.77242	7.81681	7.83193	7.83218	7.86058	7.86950
2700	7.79029	7.83328	7.84792	7.84814	7.87561	7.88423
2750	7.80730	7.84896	7.86314	7.86334	7.88993	7.89826
2800	7.82355	7.86392	7.87766	7.87783	7.90358	7.91165
2850	7.83903	7.87819	7.89152	7.89167	7.91661	7.92441
2900	7.85383	7.89181	7.90474	7.90486	7.92904	7.93660
2950	7.86797	7.90483	7.91737	7.91748	7.94091	7.94824
3000	7.88148	7.91727	7.92944	7.92953	7.95226	7.95937
3050	7.89441	7.92861	7.94098	7.94106	7.96312	7.97001
3100	7.90677	7.94000	7.95203	7.95209	7.97351	7.98019
3150	7.91862	7.95091	7.96260	7.96266	7.98345	7.98994
3200	7.92998	7.96137	7.97274	7.97277	7.99298	7.99927
3250	7.94086	7.97138	7.98245	7.98247	8.00211	8.00822
3300	7.95130	7.98099	7.99176	7.99177	8.01087	8.01681
3350	7.96132	7.99021	8.00069	8.00070	8.01927	8.02504
3400	7.97094	7.99906	8.00927	8.00926	8.02733	8.03295
3450	7.98018	8.00756	8.01750	8.01749	8.03508	8.04054
3500	7.98906	8.01573	8.02542	8.02540	8.04252	8.04784
3550	7.99761	8.02358	8.03303	8.03301	8.04968	8.05485
3600	8.00582	8.03114	8.04035	8.04031	8.05656	8.06160
3650	8.01371	8.03841	8.04739	8.04735	8.06318	8.06809
3700	8.02133	8.04541	8.05417	8.05413	8.06956	8.07434
3750	8.02867	8.05215	8.06070	8.06066	8.07570	8.08036
3800	8.03573	8.05865	8.06699	8.06694	8.08161	8.08616
3850	8.04255	8.06490	8.07305	8.07300	8.08732	8.09176
3900	8.04911	8.07094	8.07890	8.07884	8.09282	8.09715

3950	8.05544	8.07677	8.08454	8.08448	8.09812	8.10235
4000	8.06156	8.08239	8.08998	8.08992	8.10324	8.10737
4050	8.06747	8.08782	8.09524	8.09518	8.10819	8.11221
4100	8.07317	8.09306	8.10031	8.10025	8.11296	8.11690
4150	8.07868	8.09813	8.10522	8.10516	8.11758	8.12142
4200	8.08402	8.10303	8.10996	8.10989	8.12203	8.12579
4250	8.08917	8.10776	8.11454	8.11447	8.12635	8.13001
4300	8.09415	8.11234	8.11898	8.11890	8.13052	8.13410
4350	8.09898	8.11677	8.12326	8.12320	8.13455	8.13806
4400	8.10365	8.12106	8.12742	8.12734	8.13846	8.14189
4450	8.10817	8.12521	8.13143	8.13136	8.14224	8.14559
4500	8.11255	8.12924	8.13533	8.13525	8.14590	8.14919
4550	8.11679	8.13313	8.13910	8.13903	8.14945	8.15266
4600	8.12091	8.13691	8.14275	8.14268	8.15289	8.15603
4650	8.12489	8.14057	8.14630	8.14623	8.15622	8.15930
4700	8.12876	8.14412	8.14974	8.14966	8.15945	8.16247
4750	8.13250	8.14756	8.15307	8.15299	8.16259	8.16555
4800	8.13615	8.15090	8.15630	8.15623	8.16563	8.16853
4850	8.13968	8.15415	8.15944	8.15936	8.16858	8.17142
4900	8.14311	8.15730	8.16249	8.16241	8.17145	8.17423
4950	8.14644	8.16036	8.16545	8.16537	8.17423	8.17697
5000	8.14968	8.16333	8.16832	8.16825	8.17694	8.17962

SI Table 4: Vibrational heat capacity values for all peptides 0-5000K

T(K)	ondansetron	verapamil	acetaminophen	clozapine N-oxide
0	0.00000	0.00000	0.00000	0.00000
2	0.00000	0.00325	0.00000	0.00000
4	0.00032	0.03109	0.00002	0.00024
6	0.00451	0.06658	0.00077	0.00404
8	0.01536	0.09952	0.00565	0.01493
10	0.03041	0.12857	0.01754	0.03114
12	0.04683	0.15461	0.03626	0.04967
14	0.06343	0.17878	0.05982	0.06861
16	0.08003	0.20194	0.08614	0.08721
18	0.09678	0.22470	0.11360	0.10527
20	0.11387	0.24745	0.14111	0.12281
22	0.13134	0.27040	0.16805	0.13991
24	0.14918	0.29362	0.19409	0.15664
26	0.16733	0.31714	0.21902	0.17306
28	0.18572	0.34092	0.24281	0.18919

30	0.20425	0.36490	0.26547	0.20506
32	0.22285	0.38900	0.28702	0.22070
34	0.24148	0.41315	0.30754	0.23612
36	0.26007	0.43729	0.32709	0.25133
38	0.27859	0.46137	0.34572	0.26637
40	0.29703	0.48535	0.36351	0.28125
42	0.31536	0.50918	0.38056	0.29599
44	0.33357	0.53283	0.39689	0.31063
46	0.35165	0.55629	0.41261	0.32519
48	0.36961	0.57953	0.42777	0.33969
50	0.38743	0.60255	0.44244	0.35416
52	0.40512	0.62532	0.45668	0.36861
54	0.42268	0.64786	0.47056	0.38308
56	0.44011	0.67014	0.48411	0.39757
58	0.45742	0.69217	0.49740	0.41211
60	0.47461	0.71395	0.51049	0.42671
62	0.49168	0.73548	0.52342	0.44139
64	0.50864	0.75676	0.53623	0.45614
66	0.52549	0.77779	0.54895	0.47099
68	0.54223	0.79857	0.56163	0.48594
70	0.55888	0.81911	0.57432	0.50098
72	0.57543	0.83941	0.58700	0.51613
74	0.59188	0.85948	0.59974	0.53140
76	0.60824	0.87930	0.61253	0.54676
78	0.62452	0.89891	0.62542	0.56225
80	0.64072	0.91829	0.63840	0.57783
82	0.65683	0.93745	0.65151	0.59352
84	0.67286	0.95640	0.66472	0.60932
86	0.68883	0.97514	0.67809	0.62521
88	0.70472	0.99368	0.69158	0.64121
90	0.72054	1.01201	0.70523	0.65731
92	0.73631	1.03016	0.71904	0.67349
94	0.75201	1.04812	0.73298	0.68976
96	0.76766	1.06589	0.74709	0.70611
98	0.78325	1.08348	0.76133	0.72255
100	0.79879	1.10090	0.77574	0.73906
150	1.18035	1.49405	1.17407	1.16778
200	1.57167	1.84909	1.60854	1.61276
250	1.98627	2.20715	2.05295	2.06783
298.15	2.40038	2.56451	2.47854	2.50752
300	2.41638	2.57841	2.49470	2.52427

350	2.84502	2.95414	2.92140	2.96825
400	3.25630	3.32097	3.32267	3.38714
450	3.64002	3.66861	3.69244	3.77322
500	3.99173	3.99167	4.02889	4.12377
550	4.31105	4.28862	4.33311	4.43960
600	4.59989	4.56027	4.60779	4.72344
650	4.86114	4.80858	4.85619	4.97877
700	5.09789	5.03583	5.08156	5.20910
750	5.31306	5.24426	5.28684	5.41763
800	5.50920	5.43587	5.47454	5.60716
850	5.68853	5.61240	5.64679	5.78004
900	5.85293	5.77535	5.80535	5.93824
950	6.00398	5.92601	5.95168	6.08341
1000	6.14305	6.06549	6.08704	6.21695
1050	6.27130	6.19474	6.21242	6.34005
1100	6.38976	6.31465	6.32879	6.45372
1150	6.49931	6.42597	6.43689	6.55885
1200	6.60076	6.52941	6.53744	6.65621
1250	6.69480	6.62559	6.63105	6.74649
1300	6.78208	6.71509	6.71828	6.83032
1350	6.86317	6.79843	6.79963	6.90822
1400	6.93857	6.87610	6.87556	6.98071
1450	7.00876	6.94854	6.94651	7.04822
1500	7.07417	7.01616	7.01282	7.11117
1550	7.13518	7.07933	7.07488	7.16991
1600	7.19214	7.13839	7.13300	7.22479
1650	7.24538	7.19365	7.18747	7.27611
1700	7.29518	7.24541	7.23856	7.32415
1750	7.34183	7.29393	7.28651	7.36916
1800	7.38553	7.33944	7.33158	7.41137
1850	7.42655	7.38219	7.37395	7.45098
1900	7.46507	7.42235	7.41381	7.48821
1950	7.50127	7.46014	7.45137	7.52321
2000	7.53533	7.49571	7.48675	7.55617
2050	7.56740	7.52923	7.52016	7.58721
2100	7.59763	7.56084	7.55168	7.61648
2150	7.62616	7.59068	7.58147	7.64411
2200	7.65309	7.61886	7.60963	7.67021
2250	7.67854	7.64550	7.63628	7.69487
2300	7.70261	7.67072	7.66153	7.71821
2350	7.72539	7.69460	7.68546	7.74031

2400	7.74698	7.71722	7.70816	7.76125
2450	7.76744	7.73868	7.72968	7.78112
2500	7.78686	7.75904	7.75016	7.79997
2550	7.80529	7.77839	7.76960	7.81787
2600	7.82281	7.79677	7.78809	7.83490
2650	7.83948	7.81426	7.80570	7.85109
2700	7.85533	7.83090	7.82247	7.86649
2750	7.87043	7.84676	7.83846	7.88117
2800	7.88481	7.86187	7.85370	7.89516
2850	7.89853	7.87628	7.86825	7.90850
2900	7.91162	7.89004	7.88212	7.92123
2950	7.92412	7.90317	7.89540	7.93340
3000	7.93605	7.91572	7.90809	7.94502
3050	7.94747	7.92772	7.92021	7.95612
3100	7.95838	7.93920	7.93182	7.96675
3150	7.96883	7.95019	7.94295	7.97693
3200	7.97884	7.96071	7.95361	7.98667
3250	7.98843	7.97080	7.96382	7.99601
3300	7.99762	7.98047	7.97363	8.00496
3350	8.00643	7.98974	7.98304	8.01355
3400	8.01489	7.99865	7.99205	8.02179
3450	8.02302	8.00720	8.00074	8.02971
3500	8.03082	8.01541	8.00907	8.03732
3550	8.03832	8.02330	8.01709	8.04463
3600	8.04553	8.03090	8.02479	8.05166
3650	8.05247	8.03820	8.03221	8.05843
3700	8.05915	8.04523	8.03935	8.06494
3750	8.06558	8.05200	8.04623	8.07121
3800	8.07178	8.05852	8.05286	8.07725
3850	8.07774	8.06481	8.05926	8.08307
3900	8.08349	8.07088	8.06542	8.08869
3950	8.08905	8.07672	8.07137	8.09410
4000	8.09440	8.08236	8.07711	8.09933
4050	8.09958	8.08781	8.08265	8.10437
4100	8.10457	8.09307	8.08802	8.10925
4150	8.10939	8.09815	8.09319	8.11395
4200	8.11405	8.10306	8.09819	8.11850
4250	8.11856	8.10781	8.10302	8.12290
4300	8.12292	8.11240	8.10770	8.12716
4350	8.12713	8.11684	8.11223	8.13127
4400	8.13121	8.12114	8.11661	8.13525

4450	8.13516	8.12530	8.12086	8.13911
4500	8.13898	8.12933	8.12496	8.14285
4550	8.14268	8.13324	8.12895	8.14646
4600	8.14628	8.13702	8.13281	8.14997
4650	8.14976	8.14069	8.13654	8.15337
4700	8.15313	8.14425	8.14018	8.15667
4750	8.15641	8.14770	8.14370	8.15986
4800	8.15958	8.15105	8.14711	8.16296
4850	8.16266	8.15430	8.15042	8.16598
4900	8.16565	8.15745	8.15365	8.16890
4950	8.16856	8.16051	8.15677	8.17173
5000	8.17138	8.16349	8.15981	8.17449

SI Table 5: Vibrational heat capacity values for all small-molecule drugs 0-5000K

T(K)	sucrose	D-glucose
0	0.00000	0.00000
2	0.00000	0.00000
4	0.00061	0.00000
6	0.00691	0.00000
8	0.02089	0.00001
10	0.03903	0.00016
12	0.05880	0.00078
14	0.07918	0.00242
16	0.09986	0.00554
18	0.12067	0.01043
20	0.14157	0.01720
22	0.16249	0.02580
24	0.18342	0.03607
26	0.20431	0.04784
28	0.22517	0.06091
30	0.24599	0.07509
32	0.26679	0.09019
34	0.28758	0.10604
36	0.30836	0.12255
38	0.32917	0.13955
40	0.35002	0.15697
42	0.37094	0.17471
44	0.39195	0.19272
46	0.41305	0.21096

48	0.43427	0.22938
50	0.45561	0.24794
52	0.47708	0.26664
54	0.49867	0.28545
56	0.52039	0.30436
58	0.54223	0.32338
60	0.56417	0.34249
62	0.58623	0.36170
64	0.60838	0.38100
66	0.63061	0.40041
68	0.65292	0.41988
70	0.67528	0.43948
72	0.69769	0.45916
74	0.72013	0.47893
76	0.74259	0.49880
78	0.76506	0.51874
80	0.78752	0.53878
82	0.80997	0.55890
84	0.83239	0.57909
86	0.85477	0.59935
88	0.87711	0.61968
90	0.89939	0.64007
92	0.92160	0.66051
94	0.94373	0.68099
96	0.96579	0.70149
98	0.98775	0.72204
100	1.00962	0.74261
150	1.51619	1.24443
200	1.95633	1.70033
250	2.37164	2.13114
298.15	2.76786	2.54010
300	2.78301	2.55571
350	3.18655	2.97104
400	3.57095	3.36632
450	3.92749	3.73304
500	4.25235	4.06745
550	4.54559	4.36964
600	4.80946	4.64190
650	5.04711	4.88746
700	5.26183	5.10964
750	5.45663	5.31151

800	5.63414	5.49572
850	5.79658	5.66452
900	5.94575	5.81977
950	6.08318	5.96297
1000	6.21013	6.09542
1050	6.32764	6.21817
1100	6.43664	6.33214
1150	6.53787	6.43813
1200	6.63204	6.53678
1250	6.71972	6.62875
1300	6.80145	6.71454
1350	6.87773	6.79467
1400	6.94895	6.86954
1450	7.01554	6.93958
1500	7.07783	7.00514
1550	7.13616	7.06658
1600	7.19083	7.12419
1650	7.24209	7.17823
1700	7.29021	7.22900
1750	7.33542	7.27670
1800	7.37792	7.32157
1850	7.41791	7.36380
1900	7.45558	7.40359
1950	7.49107	7.44110
2000	7.52455	7.47649
2050	7.55614	7.50991
2100	7.58600	7.54148
2150	7.61422	7.57135
2200	7.64092	7.59961
2250	7.66620	7.62636
2300	7.69016	7.65172
2350	7.71288	7.67578
2400	7.73443	7.69861
2450	7.75490	7.72030
2500	7.77436	7.74091
2550	7.79286	7.76051
2600	7.81045	7.77916
2650	7.82721	7.79693
2700	7.84318	7.81386
2750	7.85841	7.83000
2800	7.87293	7.84541

2850	7.88680	7.86010
2900	7.90004	7.87414
2950	7.91270	7.88758
3000	7.92480	7.90042
3050	7.93638	7.91271
3100	7.94746	7.92446
3150	7.95808	7.93574
3200	7.96827	7.94654
3250	7.97802	7.95690
3300	7.98739	7.96684
3350	7.99637	7.97638
3400	8.00501	7.98554
3450	8.01330	7.99435
3500	8.02127	8.00281
3550	8.02894	8.01094
3600	8.03631	8.01878
3650	8.04341	8.02632
3700	8.05025	8.03358
3750	8.05683	8.04058
3800	8.06318	8.04732
3850	8.06930	8.05383
3900	8.07521	8.06009
3950	8.08091	8.06614
4000	8.08641	8.07199
4050	8.09172	8.07762
4100	8.09685	8.08307
4150	8.10181	8.08835
4200	8.10660	8.09343
4250	8.11123	8.09836
4300	8.11572	8.10313
4350	8.12006	8.10774
4400	8.12427	8.11220
4450	8.12833	8.11654
4500	8.13227	8.12072
4550	8.13610	8.12478
4600	8.13980	8.12871
4650	8.14339	8.13254
4700	8.14687	8.13623
4750	8.15025	8.13983
4800	8.15352	8.14330
4850	8.15670	8.14668

4900	8.15980	8.14997
4950	8.16280	8.15316
5000	8.16571	8.15626

SI Table 6: Vibrational heat capacity values for all sugars 0-5000K

T(K)	Agilent Tune Mix 322	Agilent Tune Mix 1222	Agilent Tune Mix 2122
0	0.00000	0.00000	0.00000
2	0.00000	0.01969	0.00578
4	0.00010	0.07428	0.04180
6	0.00316	0.13625	0.08929
8	0.01545	0.20371	0.14039
10	0.03813	0.27323	0.19266
12	0.06851	0.34202	0.24528
14	0.10409	0.40831	0.29777
16	0.14324	0.47119	0.34966
18	0.18497	0.53033	0.40052
20	0.22858	0.58576	0.45003
22	0.27350	0.63768	0.49797
24	0.31922	0.68639	0.54428
26	0.36530	0.73222	0.58894
28	0.41140	0.77552	0.63205
30	0.45718	0.81660	0.67372
32	0.50241	0.85578	0.71411
34	0.54689	0.89333	0.75337
36	0.59048	0.92952	0.79167
38	0.63308	0.96457	0.82915
40	0.67464	0.99867	0.86597
42	0.71512	1.03199	0.90224
44	0.75453	1.06468	0.93809
46	0.79288	1.09687	0.97361
48	0.83016	1.12864	1.00889
50	0.86644	1.16008	1.04399
52	0.90174	1.19127	1.07896
54	0.93610	1.22225	1.11386
56	0.96959	1.25307	1.14871
58	1.00223	1.28376	1.18355
60	1.03407	1.31434	1.21837
62	1.06515	1.34483	1.25321
64	1.09552	1.37524	1.28805

66	1.12522	1.40558	1.32290
68	1.15428	1.43585	1.35775
70	1.18273	1.46605	1.39259
72	1.21062	1.49618	1.42742
74	1.23796	1.52623	1.46222
76	1.26479	1.55621	1.49699
78	1.29113	1.58609	1.53169
80	1.31701	1.61588	1.56633
82	1.34243	1.64557	1.60089
84	1.36743	1.67515	1.63534
86	1.39202	1.70461	1.66969
88	1.41622	1.73395	1.70391
90	1.44003	1.76316	1.73800
92	1.46349	1.79223	1.77193
94	1.48658	1.82116	1.80571
96	1.50933	1.84994	1.83932
98	1.53176	1.87856	1.87275
100	1.55387	1.90702	1.90598
150	2.02407	2.55961	2.66272
200	2.39897	3.10861	3.28431
250	2.74530	3.59222	3.81661
298.15	3.07717	4.01982	4.27528
300	3.08994	4.03561	4.29202
350	3.43273	4.44434	4.72076
400	3.76460	4.81631	5.10403
450	4.07751	5.14974	5.44245
500	4.36725	5.44528	5.73847
550	4.63288	5.70564	5.99609
600	4.87548	5.93457	6.21996
650	5.09706	6.13608	6.41477
700	5.29987	6.31396	6.58479
750	5.48604	6.47161	6.73377
800	5.65744	6.61194	6.86491
850	5.81567	6.73738	6.98088
900	5.96206	6.84999	7.08389
950	6.09774	6.95147	7.17579
1000	6.22370	7.04325	7.25810
1050	6.34072	7.12653	7.33212
1100	6.44958	7.20231	7.39890
1150	6.55091	7.27146	7.45935
1200	6.64530	7.33471	7.51424

1250	6.73328	7.39270	7.56421
1300	6.81532	7.44598	7.60982
1350	6.89190	7.49502	7.65156
1400	6.96342	7.54026	7.68985
1450	7.03024	7.58205	7.72504
1500	7.09273	7.62073	7.75745
1550	7.15121	7.65657	7.78735
1600	7.20597	7.68985	7.81500
1650	7.25730	7.72080	7.84061
1700	7.30543	7.74960	7.86437
1750	7.35060	7.77646	7.88645
1800	7.39304	7.80153	7.90699
1850	7.43293	7.82496	7.92614
1900	7.47048	7.84689	7.94401
1950	7.50582	7.86744	7.96071
2000	7.53912	7.88672	7.97634
2050	7.57054	7.90482	7.99099
2100	7.60019	7.92184	8.00473
2150	7.62820	7.93785	8.01764
2200	7.65469	7.95294	8.02978
2250	7.67973	7.96717	8.04121
2300	7.70346	7.98061	8.05198
2350	7.72593	7.99330	8.06214
2400	7.74725	8.00530	8.07174
2450	7.76747	8.01666	8.08081
2500	7.78668	8.02743	8.08939
2550	7.80493	8.03763	8.09752
2600	7.82229	8.04732	8.10523
2650	7.83881	8.05652	8.11254
2700	7.85453	8.06526	8.11948
2750	7.86952	8.07358	8.12607
2800	7.88381	8.08150	8.13235
2850	7.89745	8.08904	8.13832
2900	7.91047	8.09623	8.14400
2950	7.92290	8.10309	8.14942
3000	7.93479	8.10963	8.15459
3050	7.94616	8.11589	8.15953
3100	7.95704	8.12186	8.16424
3150	7.96746	8.12758	8.16875
3200	7.97744	8.13305	8.17306
3250	7.98700	8.13828	8.17718

3300	7.99617	8.14330	8.18112
3350	8.00498	8.14811	8.18491
3400	8.01343	8.15273	8.18853
3450	8.02154	8.15715	8.19201
3500	8.02934	8.16140	8.19534
3550	8.03684	8.16549	8.19855
3600	8.04406	8.16941	8.20163
3650	8.05100	8.17318	8.20459
3700	8.05768	8.17681	8.20743
3750	8.06411	8.18031	8.21017
3800	8.07031	8.18367	8.21280
3850	8.07630	8.18691	8.21534
3900	8.08206	8.19004	8.21778
3950	8.08762	8.19305	8.22014
4000	8.09298	8.19595	8.22241
4050	8.09816	8.19876	8.22460
4100	8.10317	8.20146	8.22672
4150	8.10801	8.20407	8.22876
4200	8.11269	8.20660	8.23073
4250	8.11720	8.20904	8.23263
4300	8.12157	8.21140	8.23448
4350	8.12580	8.21368	8.23626
4400	8.12990	8.21589	8.23798
4450	8.13386	8.21802	8.23964
4500	8.13770	8.22009	8.24126
4550	8.14142	8.22209	8.24282
4600	8.14503	8.22404	8.24433
4650	8.14852	8.22592	8.24580
4700	8.15190	8.22774	8.24722
4750	8.15520	8.22951	8.24859
4800	8.15839	8.23122	8.24993
4850	8.16149	8.23289	8.25123
4900	8.16449	8.23450	8.25248
4950	8.16741	8.23607	8.25370
5000	8.17025	8.23759	8.25489

SI Table 7: Vibrational heat capacity values for all Agilent Tune Mix ions 0-5000K

T(K)	B3LYP/6-31G(d)	B3LYP/6-31G(d,p)	B3LYP/6-31+G(d,p)	M062X/6-31G(d)
0	0.00000	0.00000	0.00000	0.00000

2	0.00000	0.00000	0.00000	0.00000
4	0.00010	0.00010	0.00008	0.00007
6	0.00316	0.00314	0.00251	0.00241
8	0.01545	0.01541	0.01312	0.01285
10	0.03813	0.03796	0.03335	0.03293
12	0.06851	0.06806	0.06070	0.06000
14	0.10409	0.10324	0.09278	0.09128
16	0.14324	0.14201	0.12834	0.12507
18	0.18497	0.18348	0.16679	0.16050
20	0.22858	0.22696	0.20771	0.19715
22	0.27350	0.27190	0.25071	0.23478
24	0.31922	0.31779	0.29532	0.27319
26	0.36530	0.36415	0.34105	0.31218
28	0.41140	0.41059	0.38739	0.35157
30	0.45718	0.45675	0.43391	0.39116
32	0.50241	0.50238	0.48026	0.43077
34	0.54689	0.54725	0.52610	0.47023
36	0.59048	0.59121	0.57119	0.50940
38	0.63308	0.63416	0.61539	0.54815
40	0.67464	0.67605	0.65857	0.58641
42	0.71512	0.71681	0.70066	0.62409
44	0.75453	0.75647	0.74161	0.66113
46	0.79288	0.79501	0.78143	0.69750
48	0.83016	0.83248	0.82011	0.73319
50	0.86644	0.86890	0.85770	0.76817
52	0.90174	0.90432	0.89422	0.80246
54	0.93610	0.93879	0.92971	0.83604
56	0.96959	0.97234	0.96424	0.86893
58	1.00223	1.00504	0.99784	0.90116
60	1.03407	1.03691	1.03057	0.93274
62	1.06515	1.06803	1.06247	0.96370
64	1.09552	1.09841	1.09359	0.99405
66	1.12522	1.12811	1.12398	1.02380
68	1.15428	1.15716	1.15368	1.05300
70	1.18273	1.18561	1.18271	1.08166
72	1.21062	1.21348	1.21114	1.10979
74	1.23796	1.24080	1.23899	1.13743
76	1.26479	1.26760	1.26629	1.16459
78	1.29113	1.29390	1.29306	1.19129
80	1.31701	1.31974	1.31933	1.21754
82	1.34243	1.34513	1.34513	1.24336

84	1.36743	1.37010	1.37049	1.26878
86	1.39202	1.39466	1.39541	1.29379
88	1.41622	1.41882	1.41991	1.31842
90	1.44003	1.44260	1.44403	1.34268
92	1.46349	1.46601	1.46776	1.36658
94	1.48658	1.48908	1.49112	1.39012
96	1.50933	1.51180	1.51413	1.41333
98	1.53176	1.53419	1.53681	1.43621
100	1.55387	1.55627	1.55914	1.45877
150	2.02407	2.02631	2.03375	1.93880
200	2.39897	2.40214	2.41247	2.31815
250	2.74530	2.75042	2.76284	2.66497
298.15	3.07717	3.08472	3.09854	2.99684
300	3.08994	3.09759	3.11145	3.00962
350	3.43273	3.44286	3.45750	3.35370
400	3.76460	3.77674	3.79162	3.68836
450	4.07751	4.09108	4.10577	4.00510
500	4.36725	4.38167	4.39590	4.29915
550	4.63288	4.64770	4.66129	4.56914
600	4.87548	4.89038	4.90323	4.81590
650	5.09706	5.11181	5.12389	5.04130
700	5.29987	5.31430	5.32563	5.24756
750	5.48604	5.50006	5.51066	5.43683
800	5.65744	5.67098	5.68089	5.61100
850	5.81567	5.82870	5.83795	5.77171
900	5.96206	5.97456	5.98322	5.92036
950	6.09774	6.10971	6.11782	6.05810
1000	6.22370	6.23513	6.24272	6.18594
1050	6.34072	6.35165	6.35877	6.30472
1100	6.44958	6.46001	6.46670	6.41521
1150	6.55091	6.56085	6.56714	6.51806
1200	6.64530	6.65477	6.66070	6.61387
1250	6.73328	6.74230	6.74789	6.70319
1300	6.81532	6.82393	6.82920	6.78652
1350	6.89190	6.90011	6.90509	6.86430
1400	6.96342	6.97125	6.97595	6.93695
1450	7.03024	7.03770	7.04217	7.00487
1500	7.09273	7.09986	7.10409	7.06838
1550	7.15121	7.15801	7.16203	7.12784
1600	7.20597	7.21247	7.21629	7.18352
1650	7.25730	7.26350	7.26713	7.23572

1700	7.30543	7.31136	7.31482	7.28470
1750	7.35060	7.35629	7.35958	7.33068
1800	7.39304	7.39849	7.40163	7.37388
1850	7.43293	7.43815	7.44115	7.41450
1900	7.47048	7.47547	7.47834	7.45271
1950	7.50582	7.51061	7.51335	7.48871
2000	7.53912	7.54372	7.54635	7.52265
2050	7.57054	7.57496	7.57748	7.55466
2100	7.60019	7.60444	7.60685	7.58487
2150	7.62820	7.63229	7.63460	7.61342
2200	7.65469	7.65861	7.66083	7.64041
2250	7.67973	7.68351	7.68565	7.66595
2300	7.70346	7.70710	7.70915	7.69014
2350	7.72593	7.72944	7.73142	7.71307
2400	7.74725	7.75063	7.75253	7.73481
2450	7.76747	7.77073	7.77257	7.75544
2500	7.78668	7.78983	7.79159	7.77504
2550	7.80493	7.80797	7.80968	7.79366
2600	7.82229	7.82523	7.82688	7.81137
2650	7.83881	7.84165	7.84324	7.82823
2700	7.85453	7.85728	7.85882	7.84429
2750	7.86952	7.87218	7.87367	7.85958
2800	7.88381	7.88639	7.88783	7.87417
2850	7.89745	7.89994	7.90133	7.88810
2900	7.91047	7.91288	7.91423	7.90138
2950	7.92290	7.92524	7.92655	7.91409
3000	7.93479	7.93706	7.93832	7.92622

SI Table 8: Vibrational heat capacity values for Agilent Tune Mix 322 ion with varying basis sets and levels of theory 0-3000K

T(K)	$(Ala)_5^+$ straight-chain	$(Ala)_5^+$ alpha-helix	$(Tyr)_5^+$ straight-chain	$(Tyr)_5^+$ alpha-helix
0	0.00000	0.00000	0.00000	0.00000
2	0.00219	0.00000	0.01564	0.00784
4	0.02403	0.00008	0.06508	0.04836
6	0.05737	0.00191	0.11160	0.09921
8	0.09481	0.00847	0.15382	0.14966
10	0.13138	0.01999	0.19325	0.19605
12	0.16626	0.03537	0.23059	0.23805

14	0.19995	0.05371	0.26628	0.27631
16	0.23295	0.07440	0.30052	0.31155
18	0.26547	0.09695	0.33338	0.34429
20	0.29753	0.12092	0.36488	0.37492
22	0.32900	0.14595	0.39504	0.40374
24	0.35975	0.17169	0.42388	0.43098
26	0.38966	0.19789	0.45143	0.45683
28	0.41863	0.22433	0.47776	0.48144
30	0.44663	0.25085	0.50293	0.50494
32	0.47365	0.27732	0.52699	0.52745
34	0.49972	0.30367	0.55001	0.54907
36	0.52493	0.32983	0.57207	0.56987
38	0.54933	0.35578	0.59323	0.58995
40	0.57303	0.38148	0.61356	0.60936
42	0.59611	0.40693	0.63314	0.62818
44	0.61865	0.43214	0.65203	0.64647
46	0.64075	0.45711	0.67031	0.66430
48	0.66247	0.48185	0.68805	0.68170
50	0.68386	0.50638	0.70529	0.69874
52	0.70499	0.53071	0.72212	0.71546
54	0.72589	0.55484	0.73859	0.73192
56	0.74661	0.57880	0.75474	0.74815
58	0.76716	0.60258	0.77064	0.76419
60	0.78756	0.62621	0.78633	0.78008
62	0.80785	0.64967	0.80185	0.79585
64	0.82801	0.67298	0.81724	0.81153
66	0.84807	0.69615	0.83253	0.82714
68	0.86802	0.71917	0.84775	0.84271
70	0.88786	0.74204	0.86294	0.85826
72	0.90760	0.76476	0.87811	0.87380
74	0.92724	0.78735	0.89327	0.88934
76	0.94676	0.80978	0.90845	0.90491
78	0.96619	0.83206	0.92366	0.92051
80	0.98549	0.85420	0.93891	0.93614
82	1.00469	0.87618	0.95421	0.95182
84	1.02377	0.89801	0.96956	0.96755
86	1.04273	0.91969	0.98497	0.98334
88	1.06157	0.94122	1.00045	0.99917
90	1.08029	0.96258	1.01598	1.01507

92	1.09888	0.98379	1.03159	1.03103
94	1.11736	1.00485	1.04726	1.04705
96	1.13571	1.02574	1.06299	1.06313
98	1.15394	1.04648	1.07879	1.07926
100	1.17204	1.06706	1.09466	1.09545
150	1.59081	1.53599	1.50602	1.51373
200	1.97329	1.94751	1.93421	1.94640
250	2.35000	2.33931	2.37311	2.38689
298.15	2.71481	2.71156	2.79642	2.80982
300	2.72881	2.72576	2.81252	2.82588
350	3.10345	3.10429	3.23824	3.25018
400	3.46399	3.46686	3.63831	3.64852
450	3.80285	3.80674	4.00588	4.01439
500	4.11622	4.12060	4.33884	4.34584
550	4.40342	4.40794	4.63830	4.64403
600	4.66566	4.67010	4.90709	4.91175
650	4.90503	4.90926	5.14861	5.15241
700	5.12387	5.12782	5.36631	5.36940
750	5.32444	5.32804	5.56327	5.56578
800	5.50876	5.51199	5.74218	5.74422
850	5.67854	5.68140	5.90532	5.90697
900	5.83528	5.83777	6.05459	6.05592
950	5.98025	5.98238	6.19156	6.19262
1000	6.11453	6.11633	6.31757	6.31842
1050	6.23907	6.24056	6.43375	6.43442
1100	6.35469	6.35591	6.54108	6.54159
1150	6.46215	6.46311	6.64038	6.64076
1200	6.56210	6.56283	6.73239	6.73267
1250	6.65513	6.65566	6.81777	6.81795
1300	6.74180	6.74215	6.89707	6.89718
1350	6.82260	6.82280	6.97083	6.97088
1400	6.89799	6.89805	7.03950	7.03949
1450	6.96838	6.96832	7.10350	7.10345
1500	7.03416	7.03399	7.16320	7.16312
1550	7.09567	7.09542	7.21896	7.21884
1600	7.15324	7.15291	7.27108	7.27094
1650	7.20717	7.20677	7.31985	7.31969
1700	7.25772	7.25727	7.36552	7.36535
1750	7.30516	7.30465	7.40834	7.40815

1800	7.34970	7.34915	7.44852	7.44832
1850	7.39156	7.39098	7.48626	7.48604
1900	7.43093	7.43033	7.52173	7.52151
1950	7.46799	7.46737	7.55510	7.55488
2000	7.50291	7.50228	7.58653	7.58631
2050	7.53584	7.53519	7.61616	7.61593
2100	7.56692	7.56626	7.64410	7.64388
2150	7.59626	7.59560	7.67049	7.67026
2200	7.62401	7.62334	7.69542	7.69519
2250	7.65025	7.64958	7.71900	7.71878
2300	7.67510	7.67443	7.74132	7.74109
2350	7.69863	7.69797	7.76246	7.76224
2400	7.72096	7.72029	7.78250	7.78228
2450	7.74213	7.74147	7.80151	7.80130
2500	7.76224	7.76159	7.81956	7.81935
2550	7.78135	7.78071	7.83671	7.83650
2600	7.79952	7.79888	7.85302	7.85281
2650	7.81681	7.81618	7.86853	7.86832
2700	7.83328	7.83265	7.88330	7.88310
2750	7.84896	7.84835	7.89737	7.89717
2800	7.86392	7.86331	7.91079	7.91059
2850	7.87819	7.87760	7.92359	7.92340
2900	7.89181	7.89123	7.93580	7.93562
2950	7.90483	7.90426	7.94747	7.94729
3000	7.91727	7.91671	7.95863	7.95845

SI Table 9: Vibrational heat capacity values for penta-L-alanine and penta-L-tyrosine with varying secondary structures 0-3000K

T(K)	Lipid Average	Oligonucleotide Average	Small-Molecule Drugs Average	Peptide Average	Sugars Average	Agilent Tune Mix Average
0	0.00000	0.00000	0.00000	0.00000	0.00000	0.00000
2	0.02113	0.00639	0.00081	0.00850	0.00000	0.00849
4	0.05509	0.02118	0.00792	0.03504	0.00031	0.03873
6	0.08691	0.03531	0.01898	0.06899	0.00345	0.07624
8	0.11825	0.05313	0.03386	0.10593	0.01045	0.11985
10	0.14944	0.07577	0.05192	0.14293	0.01959	0.16801
12	0.18002	0.10216	0.07184	0.17890	0.02979	0.21861

14	0.20965	0.13092	0.09266	0.21379	0.04080	0.27006
16	0.23826	0.16088	0.11383	0.24779	0.05270	0.32136
18	0.26594	0.19120	0.13509	0.28107	0.06555	0.37194
20	0.29281	0.22132	0.15631	0.31369	0.07939	0.42146
22	0.31900	0.25092	0.17743	0.34565	0.09414	0.46972
24	0.34462	0.27980	0.19838	0.37691	0.10974	0.51663
26	0.36977	0.30791	0.21914	0.40739	0.12608	0.56216
28	0.39450	0.33523	0.23966	0.43707	0.14304	0.60632
30	0.41885	0.36180	0.25992	0.46590	0.16054	0.64917
32	0.44286	0.38768	0.27989	0.49391	0.17849	0.69076
34	0.46653	0.41293	0.29957	0.52109	0.19681	0.73120
36	0.48988	0.43762	0.31894	0.54750	0.21545	0.77055
38	0.51290	0.46182	0.33801	0.57317	0.23436	0.80893
40	0.53561	0.48558	0.35678	0.59817	0.25350	0.84642
42	0.55798	0.50897	0.37527	0.62254	0.27282	0.88312
44	0.58003	0.53202	0.39348	0.64635	0.29234	0.91910
46	0.60174	0.55478	0.41144	0.66965	0.31200	0.95445
48	0.62313	0.57728	0.42915	0.69247	0.33182	0.98923
50	0.64418	0.59955	0.44664	0.71488	0.35178	1.02350
52	0.66490	0.62161	0.46393	0.73689	0.37186	1.05732
54	0.68530	0.64350	0.48104	0.75856	0.39206	1.09074
56	0.70537	0.66523	0.49798	0.77991	0.41237	1.12379
58	0.72513	0.68682	0.51478	0.80096	0.43280	1.15651
60	0.74457	0.70828	0.53144	0.82173	0.45333	1.18893
62	0.76371	0.72962	0.54799	0.84224	0.47396	1.22106
64	0.78255	0.75086	0.56444	0.86252	0.49469	1.25294
66	0.80111	0.77200	0.58081	0.88256	0.51551	1.28457
68	0.81937	0.79305	0.59709	0.90239	0.53640	1.31596
70	0.83737	0.81403	0.61332	0.92202	0.55738	1.34713
72	0.85510	0.83493	0.62949	0.94144	0.57842	1.37807
74	0.87257	0.85576	0.64562	0.96068	0.59953	1.40881
76	0.88978	0.87653	0.66171	0.97974	0.62069	1.43933
78	0.90676	0.89723	0.67777	0.99862	0.64190	1.46964
80	0.92350	0.91788	0.69381	1.01734	0.66315	1.49974
82	0.94001	0.93847	0.70983	1.03589	0.68443	1.52963
84	0.95631	0.95901	0.72582	1.05429	0.70574	1.55931
86	0.97239	0.97950	0.74182	1.07253	0.72706	1.58877
88	0.98826	0.99993	0.75780	1.09063	0.74840	1.61803
90	1.00394	1.02032	0.77377	1.10860	0.76973	1.64706
92	1.01943	1.04065	0.78975	1.12642	0.79105	1.67588
94	1.03473	1.06094	0.80572	1.14412	0.81236	1.70448

96	1.04985	1.08118	0.82169	1.16170	0.83364	1.73286
98	1.06480	1.10138	0.83765	1.17915	0.85490	1.76102
100	1.07959	1.12153	0.85362	1.19649	0.87611	1.78896
150	1.41188	1.61187	1.25406	1.60458	1.38031	2.41547
200	1.72153	2.08518	1.66052	1.99264	1.82833	2.93063
250	2.05268	2.55132	2.07855	2.38139	2.25139	3.38471
298.15	2.39831	2.99115	2.48774	2.75803	2.65398	3.79076
300	2.41197	3.00775	2.50344	2.77246	2.66936	3.80586
350	2.78505	3.44406	2.92220	3.15726	3.07880	4.19928
400	3.15414	3.85020	3.32177	3.52541	3.46864	4.56165
450	3.50632	4.22043	3.69357	3.86954	3.83027	4.88990
500	3.83488	4.55345	4.03402	4.18623	4.15990	5.18367
550	4.13775	4.85096	4.34309	4.47519	4.45761	5.44487
600	4.41553	5.11623	4.62285	4.73797	4.72568	5.67667
650	4.67007	5.35307	4.87617	4.97694	4.96729	5.88263
700	4.90360	5.56520	5.10610	5.19467	5.18573	6.06621
750	5.11828	5.75596	5.31545	5.39359	5.38407	6.23048
800	5.31608	5.92825	5.50669	5.57588	5.56493	6.37810
850	5.49867	6.08449	5.68194	5.74337	5.73055	6.51131
900	5.66752	6.22674	5.84297	5.89766	5.88276	6.63198
950	5.82385	6.35667	5.99127	6.04008	6.02308	6.74167
1000	5.96876	6.47570	6.12813	6.17179	6.15277	6.84168
1050	6.10320	6.58504	6.25463	6.29376	6.27291	6.93312
1100	6.22802	6.68570	6.37173	6.40687	6.38439	7.01693
1150	6.34399	6.77856	6.48026	6.51188	6.48800	7.09391
1200	6.45179	6.86436	6.58095	6.60947	6.58441	7.16475
1250	6.55208	6.94378	6.67448	6.70024	6.67424	7.23006
1300	6.64544	7.01740	6.76144	6.78475	6.75800	7.29037
1350	6.73240	7.08573	6.84236	6.86350	6.83620	7.34616
1400	6.81346	7.14925	6.91773	6.93694	6.90925	7.39784
1450	6.88907	7.20834	6.98801	7.00549	6.97756	7.44577
1500	6.95966	7.26340	7.05358	7.06951	7.04149	7.49030
1550	7.02561	7.31476	7.11483	7.12938	7.10137	7.53171
1600	7.08727	7.36271	7.17208	7.18539	7.15751	7.57028
1650	7.14497	7.40753	7.22566	7.23786	7.21016	7.60624
1700	7.19901	7.44947	7.27583	7.28703	7.25961	7.63980
1750	7.24967	7.48876	7.32286	7.33316	7.30606	7.67117
1800	7.29719	7.52559	7.36698	7.37647	7.34974	7.70052
1850	7.34182	7.56016	7.40842	7.41717	7.39085	7.72801
1900	7.38376	7.59264	7.44736	7.45545	7.42958	7.75379
1950	7.42321	7.62317	7.48400	7.49149	7.46608	7.77799

2000	7.46035	7.65192	7.51849	7.52544	7.50052	7.80073
2050	7.49534	7.67900	7.55100	7.55745	7.53303	7.82212
2100	7.52834	7.70454	7.58166	7.58766	7.56374	7.84225
2150	7.55948	7.72864	7.61060	7.61619	7.59278	7.86123
2200	7.58890	7.75140	7.63795	7.64315	7.62027	7.87914
2250	7.61672	7.77292	7.66380	7.66866	7.64628	7.89604
2300	7.64303	7.79329	7.68827	7.69281	7.67094	7.91202
2350	7.66795	7.81257	7.71144	7.71570	7.69433	7.92712
2400	7.69157	7.83085	7.73340	7.73739	7.71652	7.94143
2450	7.71396	7.84818	7.75423	7.75798	7.73760	7.95498
2500	7.73521	7.86463	7.77401	7.77752	7.75763	7.96783
2550	7.75540	7.88026	7.79279	7.79610	7.77668	7.98003
2600	7.77458	7.89511	7.81064	7.81376	7.79481	7.99161
2650	7.79283	7.90924	7.82763	7.83057	7.81207	8.00262
2700	7.81020	7.92269	7.84380	7.84657	7.82852	8.01309
2750	7.82675	7.93550	7.85920	7.86182	7.84420	8.02306
2800	7.84251	7.94772	7.87389	7.87637	7.85917	8.03255
2850	7.85755	7.95937	7.88789	7.89024	7.87345	8.04160
2900	7.87190	7.97049	7.90125	7.90348	7.88709	8.05023
2950	7.88560	7.98111	7.91402	7.91613	7.90014	8.05847
3000	7.89870	7.99126	7.92622	7.92823	7.91261	8.06634
3050	7.91122	8.00096	7.93788	7.93970	7.92454	8.07386
3100	7.92319	8.01025	7.94904	7.95076	7.93596	8.08105
3150	7.93466	8.01913	7.95972	7.96136	7.94691	8.08793
3200	7.94563	8.02765	7.96996	7.97152	7.95740	8.09451
3250	7.95615	8.03580	7.97976	7.98125	7.96746	8.10082
3300	7.96624	8.04363	7.98917	7.99058	7.97711	8.10687
3350	7.97591	8.05113	7.99819	7.99954	7.98637	8.11267
3400	7.98520	8.05834	8.00685	8.00814	7.99527	8.11823
3450	7.99412	8.06526	8.01517	8.01639	8.00382	8.12357
3500	8.00268	8.07190	8.02315	8.02433	8.01204	8.12870
3550	8.01092	8.07830	8.03083	8.03196	8.01994	8.13362
3600	8.01884	8.08444	8.03822	8.03930	8.02755	8.13836
3650	8.02646	8.09035	8.04533	8.04636	8.03486	8.14292
3700	8.03379	8.09605	8.05217	8.05316	8.04191	8.14731
3750	8.04085	8.10153	8.05875	8.05971	8.04871	8.15153
3800	8.04765	8.10681	8.06510	8.06601	8.05525	8.15560
3850	8.05421	8.11190	8.07122	8.07210	8.06156	8.15952
3900	8.06053	8.11681	8.07712	8.07796	8.06765	8.16329
3950	8.06662	8.12155	8.08281	8.08362	8.07353	8.16694
4000	8.07251	8.12612	8.08830	8.08908	8.07920	8.17045

4050	8.07819	8.13053	8.09360	8.09435	8.08467	8.17384
4100	8.08367	8.13479	8.09872	8.09944	8.08996	8.17712
4150	8.08897	8.13891	8.10367	8.10436	8.09508	8.18028
4200	8.09409	8.14289	8.10845	8.10912	8.10002	8.18334
4250	8.09904	8.14673	8.11307	8.11372	8.10480	8.18629
4300	8.10383	8.15045	8.11754	8.11816	8.10943	8.18915
4350	8.10846	8.15406	8.12187	8.12247	8.11390	8.19191
4400	8.11294	8.15754	8.12605	8.12664	8.11823	8.19459
4450	8.11728	8.16092	8.13011	8.13067	8.12243	8.19717
4500	8.12149	8.16418	8.13403	8.13458	8.12650	8.19968
4550	8.12556	8.16735	8.13783	8.13836	8.13044	8.20211
4600	8.12950	8.17041	8.14152	8.14203	8.13425	8.20447
4650	8.13333	8.17339	8.14509	8.14559	8.13796	8.20675
4700	8.13704	8.17627	8.14856	8.14903	8.14155	8.20896
4750	8.14063	8.17907	8.15192	8.15238	8.14504	8.21110
4800	8.14412	8.18178	8.15517	8.15562	8.14841	8.21318
4850	8.14751	8.18442	8.15834	8.15877	8.15169	8.21520
4900	8.15080	8.18697	8.16141	8.16183	8.15488	8.21716
4950	8.15399	8.18946	8.16439	8.16480	8.15798	8.21906
5000	8.15709	8.19187	8.16729	8.16769	8.16099	8.22091

SI Table 10: Average vibrational heat capacity values for each biomolecular ion class 0-5000K

Bibliography

1. Konc, Janez, and Dušanka Janežič. “Protein Binding Sites for Drug Design.” Biophysical Reviews 14, no. 6 (December 9, 2022): 1413–21. https://doi.org/10.1007/s12551-022-01028-3.

2. Christofi, Emilia, and Perdita Barran. “Ion Mobility Mass Spectrometry (IM-MS) for Structural Biology: Insights Gained by Measuring Mass, Charge, and Collision Cross Section.” *Chemical Reviews* 123, no. 6 (March 22, 2023): 2902–49. https://doi.org/10.1021/acs.chemrev.2c00600.

3. Price, William D., and Evan R. Williams. “Activation of Peptide Ions by Blackbody Radiation: Factors That Lead to Dissociation Kinetics in the Rapid Energy Exchange Limit.” The Journal of Physical Chemistry A 101, no. 47 (November 1, 1997): 8844–52. https://doi.org/10.1021/jp9722418.

4. Smyth, M S, and J H J Martin. “X Ray Crystallography.” *Molecular Pathology* 53, no. 1 (February 2000): 8–14.

5. Milne, Jacqueline L. S., Mario J. Borgnia, Alberto Bartesaghi, Erin E. H. Tran, Lesley A. Earl, David M. Schauder, Jeffrey Lengyel, Jason Pierson, Ardan Patwardhan, and Sriram Subramaniam. “Cryo-Electron Microscopy: A Primer for the Non-Microscopist.” The FEBS Journal 280, no. 1 (January 2013): 28–45. https://doi.org/10.1111/febs.12078.

6. Zia, Komal, Talal Siddiqui, Saqib Ali, Imran Farooq, Muhammad Sohail Zafar, and Zohaib Khurshid. “Nuclear Magnetic Resonance Spectroscopy for Medical and Dental Applications: A Comprehensive Review.” *European Journal of Dentistry* 13, no. 1 (February 2019): 124–28. https://doi.org/10.1055/s-0039-1688654.

7. Donor, Micah T., Samantha O. Shepherd, and James S. Prell. “Rapid Determination of Activation Energies for Gas-Phase Protein Unfolding and Dissociation in a Q-IM-ToF Mass Spectrometer.” Journal of the American Society for Mass Spectrometry 31, no. 3 (March 4, 2020): 602–10. https://doi.org/10.1021/jasms.9b00055.

8. “SYNAPT G2-Si Mass Spectrometry | Waters.” Waters Corporation. https://www.waters.com/waters/en_US/SYNAPT-G2-Si-Mass-Spectrometry/nav.htm?cid=134740653&locale=-.

9. Price, William D., Paul D. Schnier, and Evan R. Williams. “Tandem Mass Spectrometry of Large Biomolecule Ions by Blackbody Infrared Radiative Dissociation.” Analytical Chemistry 68, no. 5 (March 1, 1996): 859–66. https://doi.org/10.1021/ac951038a.

10. Wells, J. Mitchell, and Scott A. McLuckey. “Collision-Induced Dissociation (CID) of Peptides and Proteins.” Methods in Enzymology 402 (2005): 148–85. https://doi.org/10.1016/S0076-6879(05)02005-7.

11. Ruotolo, Brandon T., Suk-Joon Hyung, Paula M. Robinson, Kevin Giles, Robert H. Bateman, and Carol V. Robinson. “Ion Mobility–Mass Spectrometry Reveals Long-Lived, Unfolded Intermediates in the Dissociation of Protein Complexes.” *Angewandte Chemie International Edition* 46, no. 42 (October 22, 2007): 8001–4. https://doi.org/10.1002/anie.200702161.

12. Armentrout, P. B. “Threshold Collision-Induced Dissociations for the Determination of Accurate Gas-Phase Binding Energies and Reaction Barriers.” In Modern Mass Spectrometry, edited by Christoph A. Schalley, 233–62. Berlin, Heidelberg: Springer, 2003. https://doi.org/10.1007/3-540-36113-8_7.

13. Gadkari, Varun V., Brock R. Juliano, Christopher S. Mallis, Jody C. May, Ruwan T. Kurulugama, John C. Fjeldsted, John A. McLean, David H. Russell, and Brandon T. Ruotolo. “Performance Evaluation of In-Source Ion Activation Hardware for Collision-Induced Unfolding of Proteins and Protein Complexes on a Drift Tube Ion Mobility-Mass Spectrometer.” Analyst 148, no. 2 (January 16, 2023): 391–401. https://doi.org/10.1039/D2AN01452A.

14. Uggerud, Einar, and Peter J. Derrick. “Theory of Collisional Activation of Macromolecules. Impulsive Collisions of Organic Ions.” The Journal of Physical Chemistry 95, no. 3 (February 1, 1991): 1430–36. https://doi.org/10.1021/j100156a073.

15. Chandler, David. *Introduction to Modern Statistical Mechanics*. New York: Oxford University Press, 1987.

16. Gómez J, Hilser VJ, Xie D, Freire E. The heat capacity of proteins. Proteins. 1995 Aug;22(4):404-12. doi: 10.1002/prot.340220410. PMID: 7479713

17. Privalov, P.L., and G.I. Makhatadze. “Heat Capacity of Proteins: II. Partial Molar Heat Capacity of the Unfolded Polypeptide Chain of Proteins: Protein Unfolding Effects.” Journal of Molecular Biology 213, no. 2 (May 20, 1990): 385–91. https://doi.org/10.1016/S0022-2836(05)80198-6.

18. K.K. Irikura, THERMO.PY, National Institute of Standards and Technology, 2020.

19. Beyer, Terry, and D. F. Swinehart. “Algorithm 448: Number of Multiply-Restricted Partitions.” Communications of the ACM 16, no. 6 (June 1, 1973): 379. https://doi.org/10.1145/362248.362275.

20. Di Giacomo, Francesco. “A Short Account of RRKM Theory of Unimolecular Reactions and of Marcus Theory of Electron Transfer in a Historical Perspective.” Journal of Chemical Education 92, no. 3 (March 10, 2015): 476–81. https://doi.org/10.1021/ed5001312.

21. Mansell, Adam, David Kahle, and Darrin Bellert. “Calculating RRKM Rate Constants from Vibrational Frequencies and Their Dynamic Interpretation « The Mathematica Journal.” Accessed April 21, 2024. https://www.mathematica-journal.com/2017/09/26/calculating-rrkm-rate-constants-from-vibrational-frequencies-and-their-dynamic-interpretation/.

22. Kohout, Jan. “Modified Arrhenius Equation in Materials Science, Chemistry and Biology.” Molecules 26, no. 23 (November 26, 2021): 7162. https://doi.org/10.3390/molecules26237162.

23. Gillis, Elizabeth A. L., Maria Demireva, Mohammed G. Sarwar, Michael G. Chudzinski, Mark S. Taylor, Evan R. Williams, and Travis D. Fridgen. “Structure and Energetics of Gas Phase Halogen-Bonding in Mono-, Bi-, and Tri-Dentate Anion Receptors as Studied by BIRD.” *Physical Chemistry Chemical Physics* 15, no. 20 (May 1, 2013): 7638–47. https://doi.org/10.1039/C3CP00105A.

24. Moosavi, Seyed Mohamad, Balázs Álmos Novotny, Daniele Ongari, Elias Moubarak, Mehrdad Asgari, Özge Kadioglu, Charithea Charalambous, et al. “A Data-Science Approach to Predict the Heat Capacity of Nanoporous Materials.” Nature Materials 21, no. 12 (December 2022): 1419–25. https://doi.org/10.1038/s41563-022-01374-3.

25. Laidler, Keith J., and M. Christine King. “Development of Transition-State Theory.” *The Journal of Physical Chemistry* 87, no. 15 (July 1, 1983): 2657–64. https://doi.org/10.1021/j100238a002.

26. Gross, Deborah S., Yuexing Zhao, and Evan R. Williams. “Dissociation of Heme–Globin Complexes by Blackbody Infrared Radiative Dissociation: Molecular Specificity in the Gas Phase?” Journal of the American Society for Mass Spectrometry 8, no. 5 (May 1997): 519–24. https://doi.org/10.1016/S1044-0305(97)00010-X.

27. Price, William D., Paul D. Schnier, Rebecca A. Jockusch, Eric F. Strittmatter, and Evan R. Williams. “Unimolecular Reaction Kinetics in the High-Pressure Limit without Collisions.” Journal of the American Chemical Society 118, no. 43 (October 30, 1996): 10640–44. https://doi.org/10.1021/ja961812r.